UNIVERSITY OF NAPLES FEDERICO II

PhD THESIS IN MATERIALS ENGINEERING AND STRUCTURES

XXVI CYCLE

"ROLE OF NANOPARTICLE CELL-INTERFACE ON MEMBRANE CROSSING AND CYTOTOXICITY "

Tutor:
Prof. Paolo Antonio Netti
Dr. Daniela Guarnieri

Candidate:
Ornella Muscetti

Coordinator:
Prof. Giuseppe Mensitieri

April 2011-April 2014

A Sofia, Massimo e ai miei genitori

CONTENTS

ABSTRACT

Understanding the interactions of nanoparticles (NP) with the cell membrane and their trafficking through the cells is very relevant to fully explore the use of NP for efficient delivery of therapeutics and to reduce their cytotoxicity. Despite numerous efforts to establish a structure–function relationship between NP physico-chemical properties and their interactions with biological systems, the possibility to predict the fate of NP remains still far.

In this thesis we assume that the way by which NP cross the cell membrane dictates their fate. To test this hypothesis, first, we studied the effect of NP delivery across cell membrane in controlling metal-containing NP (MNP) toxicity. In particular, we delivered MNP across the cell membrane directly inside the cytosol by using a pneumatic method -a gene gun - thus bypassing the formation of endocytic vesicles. We found that the cytotoxicity of MNP is strictly reliant upon the pathway of cellular membrane crossing and their localization. In particular, if otherwise toxic MNP are allow to enter the cell bypassing any form of active-dependent mechanism as endocytosis, no significant cytotoxic effect is showed.

Starting from these results, we designed surface decorated NP by using a bio-inspired approach in order to control NP entrance and to escape the lysosomal pathway. The results show that the decoration of polystyrene NP with Herpes simplex virus type one derived gH-625 peptide affected NP intracellular distribution by reducing NP accumulation within the lysosomes, increasing intracellular free “random walk” behavior, reducing NP toxicity and enhancing blood-brain barrier crossing.

1. INTRODUCTION

1.1. Nanotechnologies

In the last decades, the progress in biochemistry, physical chemistry, microscopy and engineering have resulted in a significant interest in the properties of very small particles and their possible applications in a wide variety of fields from industrial to medical.[1]This growing interest, supported by the fast progress of technical methods based on the manipulation of the material at the atomic level, has allowed the development of a multidisciplinary science called nanotechnology[2].

Nanotechnology is considered a branch of science and technology. The National Nanotechnology Initiative of the National Science Foundation defines this science as "the understanding and control of matter at dimensions of roughly 1 to 100 nanometres (nm), where unique phenomena enable novel applications".[3] The concept based on the use of nanotechnology is that material itself can change its optical, mechanical and chemical properties at various size scale. For example, carbon has different chemical properties if their atoms are assembled in nanotubes. From this innovative point of view, it is possible to create new functional materials, tools and products with special chemical and physical characteristics. Examples of applications of nanostructured materials include self-cleaning surfaces, cosmetics containing nanoparticles, improvements in construction materials and more.[3]

Functionalized products made through the use of nanotechnology find a wide variety of applications, in fact it has been estimated a rapid grow of the market[4].

Furthermore, the scientific interest is supported by the possibility of applying nanomaterial in diagnostic and therapeutic fields. In diagnostic, the specificity and sensitivity of magnetic resonance imaging can be greatly improved by using nanoparticles (NP) as contrast enhancement material.

Concerning therapeutic field, NP used for drug delivery represent a valid alternative to traditional way of drug administration, in fact, by using NP it is possible obtain biologic effect of drugs on a specific type of cell[5].

1.2. Nanotechnologies to overcome blood brain barrier

In order to develop more effective and efficient systems for the transport of drugs in specific tissues, many researchers are studying the possibility of using NP. In particular, a specific field of nanotechnology applied to the central nervous system (CNS) is now growing up[6]. In fact, the progressive increase of the number of individuals affect by CNS diseases, has allowed the development of new strategies for enhancing drug delivery to the brain. Despite many efforts, treatments to target CNS remain still limited due to the inability of therapeutic agents to effectively reach the brain[7.] To achieve efficient treatments of the CNS related pathology, it is necessary to transport therapeutic agents across the specialized cells forming the vascular system of the brain, the blood-brain barrier (BBB).[8]Brain endothelial cells are characterized by an high expression of junction proteins and selective pathways, in this way, BBB is able to protect the brain from toxic substances, on the other hand, this selectivity represents the main obstacle for penetration of most CNS drug candidates. Currently, the strategies in use to target drugs to the CNS involve invasive treatments as intracerebral implantation of controlled release implants, intaventricula infusion of drugs directly to the CNS and BBB disruption by osmotic agents. However these approaches cause several undesirable effects in humans[9],including physiological stress and transient increase in intracranial pressure. Furthermore, destroying the BBB temporarily leaves the brain vulnerable to infection and damage from toxins, also, substances that circulate in the peripheral blood, as albumin, can have deleterious effects if they enter the brain. Most importantly a large part

of these treatments have low efficacy due to limited diffusion of drug to the surrounding tissue[10]. The diffusion of drugs from the blood into the brain depends mainly upon their ability to cross lipid membranes. Therefore, drugs of interests may not have the requisite physicochemical characteristics necessary to successfully overcome BBB. This is the reason why several strategies have been developed to overcome the BBB.[11]

A promising strategy to improve delivery of drugs to the central nervous system (CNS), is represented by the use of NP. NP are defined as particulate dispersions or solid particles with a size in the range of 1-100 nm. Depending on the method of preparation of NP, it is possible to obtain "nanocapsules", where the drug is encapsulated within a cavity formed by a single polymer membrane, or "nanospheres", where the drug is linked physically to the surface.[12]

The growing interest in these new types of materials is due to the physical-chemical properties, such as their size, electric charge and the possibility of being functionalized with multiple copies of drug molecule of interest, which play a fundamental role in the behavior of NP. Actually the major goals in designing NP as a delivery system are to control particle size, electric charge, surface functionalization and release of pharmacologically active agents in order to achieve the site-specific action of the drug at the therapeutically optimal rate and dose regimen[12-13]. These properties make nanoparticles an efficient drug delivery system that can be easily adapted to deliver drugs to various compartment of the body, including the brain, and then an attractive alternative to existing methods for transporting drugs across BBB.

By the use of NP, minimizing undesirable side effects, the drug can be transported to the place of action, in addition, encapsulating drug, NP can act protecting it from rapid degradation or clearance and enhances drug concentration in target tissues, in this way, lower doses of drug are required[14]. This modern form of therapy is especially important when there is a

discrepancy between a dose and concentration of a drug and its therapeutic results or toxic effects.[14]

Even if, it is well established the potential role of using NP in drug delivery applications, few are the NP in clinical trials. In fact, despite numerous efforts to establish a structure–function relation between the physical and chemical properties of NP and their interactions with biological systems, the way to predict their toxicological profile remains still far.

1.3. Interaction at nanoparticle-cell interface in biological system and cytotoxicity

Rapid growth in nanotechnology field is increasing the types of NP that are under development for therapeutic applications. NP interacting with serum proteins, cell membrane, DNA and organelles, establish a series of nanoparticles/biological interface that influence the way of interactions and crossing of cell membrane, the intracellular uptake, and the consequent intracellular reactions that could have biocompatible or cytotoxic outcomes[1516].

To be able to take advantages from the use of NP for drug delivery systems, it is essential to clarify how the interaction at nano-bio interface influence behaviour of NP[14].

The bio-nano interface comprises dynamically interacting components as the nanoparticle surface, that are the characteristics of which are determined by its physicochemical composition and the solid-liquid interface (Figure 1) changes that occur when the particles interact with proteins components of surrounding medium.

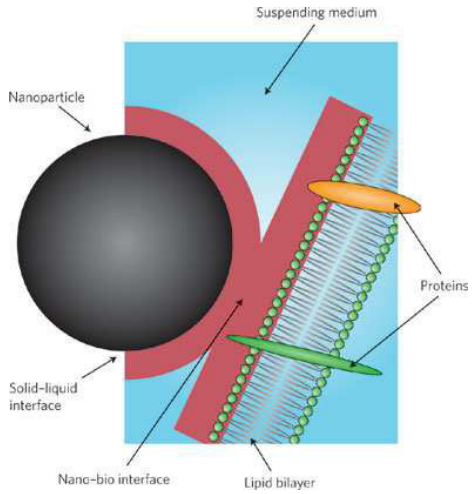

Figure.1 Representation of the interface between a nanoparticle and a lipid bilayer. Modification of the surface properties of those materials through interactions with proteins of the resuspending medium, and the dynamic interactions of the solid-liquid interface with biological molecules and cellular comprtments.(Verma et. Al, Nature materials 2008.)

Once in biological fluid, NP are quickly covered by proteins of cell culture medium that form the so called "protein corona[17].The composition of the protein corona depends upon NP physico-chemical properties and determines interactions with cell membrane[18].Interactions between NP and cell membrane may trigger cell crossing and NP fate. It has been shown that 50 nm silica NP have high energy of the bare surface and adsorb strongly to cell membranes because of unspecific interactions; this lead to strong damage to cells when exposed in the absence of serum. In the presence of serum proteins, however, the formation of a protein corona has already lowered the surface energy and unspecific interactionsbetween the NP-corona complex and the cell membrane are much reduced. In this way, in the presence of serum, the damage is mitigated; this effect can be related to the adhesion properties of the NP in the two conditions.

1.3.1. Mechanisms of cytotoxicity

The influence of multiple parameters on the cytotoxicity of NP leads to the identification of common principles of toxic action, these could be helpful in the identification of toxic NP and to predict toxicity effects. Generation of reactive oxygen species (ROS) and action by dissolved ions were identified as common mechanisms for metal containing NP (MNP)[19-20].Moreover, interactions with proteins are involved in the cytotoxicity of NP, both by changing their physico-chemical parameters and as targets for cytotoxicity.

2.1.1. Reactive oxygen species (ROS) generation

Reactive oxygen species are defined as molecules containing one or more oxygen atoms, which are more reactive than molecular oxygen. The most common ROS are superoxide radical, hydroperoxyl radical, hydroxyl radical, nitric oxide, and hydrogen peroxide. ROS originate in the cell mainly from enzymatic activity of myeloperoxidase and cytochrome P450 enzymes, oxidases and flavoproteins in the peroxisomes, of NADPH oxidase at the plasma membrane, of cytoplasmic xanthine oxidase, from autooxidation of hemoglobin (Fenton reaction), riboflavin and catecholamines, transient metals, and from the electron transport chain of the mitochondria (Figure 2.a.). External factors for ROS generation include photoactivation and particle dissolution. In physiological concentrations, ROS are important regulators of cellular processes, such as growth, survival, proliferation, cell cycle arrest, apoptosis, differentiation, migration of cells, inflammation, and changes of extracellular matrix. Pathologically increased ROS cause oxidative damage of lipid (lipid peroxidation), protein (modification of amino acids, fragmentation and aggregation of proteins) and DNA (mutations and altered gene transcription) (Figure 2.b.). When intracellular levels of ROS rise to pathological concentrations antioxidant enzymes such as heme

oxygenase 1, superoxide dismutase, catalase, and glutathione peroxidase are induced as the first line of defense. At higher ROS levels activation of pro-inflammatory signaling pathways, such as the JNK and NF-κB cascades, occurs. Higher and more prolonged oxidative stress levels induce cellular perturbation and result in a decrease in mitochondrial membrane potential, leading to cell death[22].

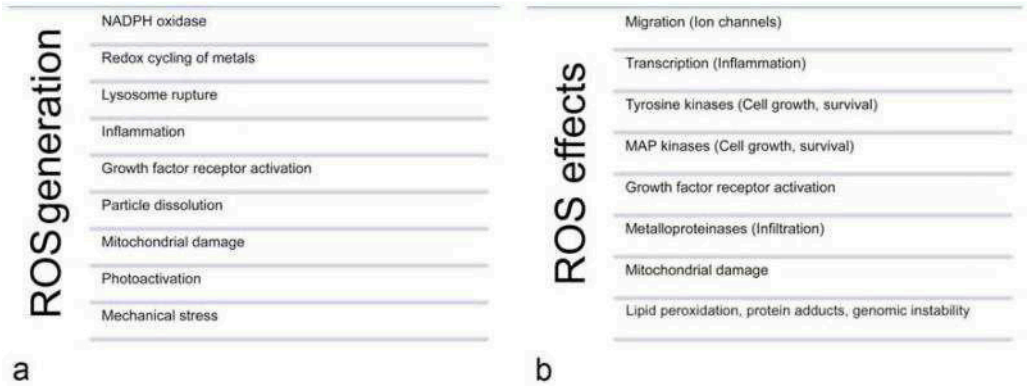

Figure 2. Sources (a) and cellular effects (b) of reactive oxygen species (ROS). (Xia t, et al., Nano letters, 2006)

NP may increase ROS levels by depletion of ROS scavengers (for instance by binding to these scavenger molecules), by reactivity at the NP surface, and by influencing intracellular production, e.g. by interaction of NP with lysosomes and mitochondria. Cu, TiO_2, and iron oxide NP produce ROS in cellular systems[22- 23]. Metallic NP may generate ROS by two types of reactions inside the cells. The Fenton-type reaction describes the reaction of metal ions with hydrogen peroxide to produce an oxidized metal ion and a hydroxide radical. The Haber-Weiss-type reaction involves an oxidized metal ion, reduced by superoxide, and hydrogen peroxide to generate oxidized metal ions and hydroxyl radical[24].

Mitochondria as targets for NP can aggravate cytotoxicity by increasing intracellular ROS-levels. Morphological and biochemical studies show that several types of NP can damage mitochondria by causing morphological alterations (swelling of mitochondria) or decrease of the mitochondrial

membrane potential[25]. Increased mitochondrial membrane permeability caused by mechanical disruption, through disturbance of the respiratory chain, and through changes in Bax and Bcl-2 expression, as a consequence of the greater mitochondrial membrane permeability cytochrome C as initiator of the intrinsic (mitochondrial) way of apoptosis is released. Impairment of mitochondrial function can also be caused by decreased production or down-regulation of mitochondrial DNA-encoded proteins. Furthermore, mitochondria cross talk with the endoplasmic reticulum by Bcl-2 proteins and Ca^{2+}-signalling. Endoplasmic reticulum stress has been shown to be involved in cytotoxicity caused by Ag NP and SiO_2 NP[26].

2.1.2 Metal ions release

Quantum dots, Ag, ZnO, and iron oxide NP, presumably act predominantly by free ions. When NP are dissolved, intracellular concentrations can rise. Cytosolic and mitochondrial Zn^{2+} concentrations, for instance, increase significantly[27] at NP sizes of <50 nm. Increased Zn^{2+} concentrations inhibit cellular respiration[28], and Ag^{+} ions act on the same sites as Ca^{2+} resulting in an increase of Ca^{2+} from sarcoplasmic reticulum[29]. Release of metal ions can also influence gene transcription. Iron response elements are present on transferrin receptor mRNA and on ferritin mRNA and allow binding of iron response element binding proteins. Iron blocks the binding in these proteins and leads to degradation of mRNA for the receptor[30]. Iron ions released from iron oxide particles by this mechanism can reduce translation of transferrin receptor mRNA.

2.1.3 Lysosome impairment

Lysosomes are obvious targets for NP since many types of NP (iron oxide, polystyrene, Au, quantum dots) are taken up by endocytosis and stored in lysosomes[31]. In addition to accumulation, NP have been reported to cause destabilization of lysosomes and permeabilization of lysosomal membranes[32-33]. Partial lysosomal membrane permeabilization results in ROS generation and apoptotic cell death, while massive permeabilization induces cytosolic acidification and necrosis. Interference of NP with lysosomes can result in oxidative cell damage by ROS, mitochondrial damage, and decreased elimination of macromolecules (lysosomal dysfunction) and of damaged organelles (reduced autophagy) from the cells. Storage of both MNP and PS NP in lysosomes was accompanied by morphological damage, such as swelling and also destruction. Furthermore, NP can interact with lysosomal membranes and increase lysosomal permeability [34]. It has been well established that, once in contact with biological fluid such as culture medium, NP are quickly covered by a layer of biomolecules that form the protein corona, which confers a new identity to the NP[35]. In particular, Dawson at al. have demonstrated in human brain astrocytoma cell line, effects of loss of protein corona on the toxicity consequential response of cell to 50 nm aminated polystyrene NP (PS NP NH2 50 nm) uptake, in fact, upon their internalization, PS NP NH2 50 nm, accumulate in the lysosomes, like several other NP of different size and materials. Once in the lysosomes, NP'corona is degraded by the protolithic enzymes, and the exposition of the positive charge cause a strong lysosomal swelling, followed by membrane damage witch lead to the cytosolic release of lysosomal content, and finally apoptosis (Figure3). The same results have been also reported for silica and PLGA NP in human brain derived endotheilial cells [35.]

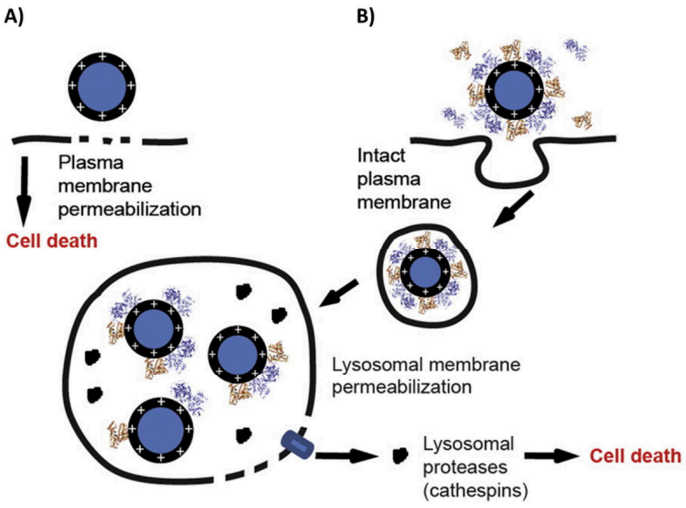

Figure 3. Loss of protein corona and its effect on lysosome. The protein corona screens the positive charges of the PS-NH2 nanoparticles and delays their impact on cells. Schematic representation of the impact of PS-NH2 nanoparticles. In absence of serum proteins PS-NH2 nanoparticles damages the cell membrane leading to quick cell membrane permeabilisation(A); in the presence of serum , PS-NH2 nanoparticles get covered by a protein corona which screens their positive charges, thus the corona is retained during nanoparticle uptake and until trafficked to the lysosomes. In the lysosomes the corona is degraded and the positive charge of the PS-NH2 nanoparticle leads to lysosomal membrane permeabilization and ultimately cell death (B). (Fenjuan et al., Nanomedicine, 2013)

The alteration of lysosomal function is associated to the proton sponge effect. In fact, the positive charge on NP surface is able of sequestering protons, the proton pump on lysosome membrane lead to the retention of one anion Cl- and one water molecule for each proton that enter the lysosome with a consequence influx of water. This is the process that causes the membrane swelling and rupture (Figure 4).

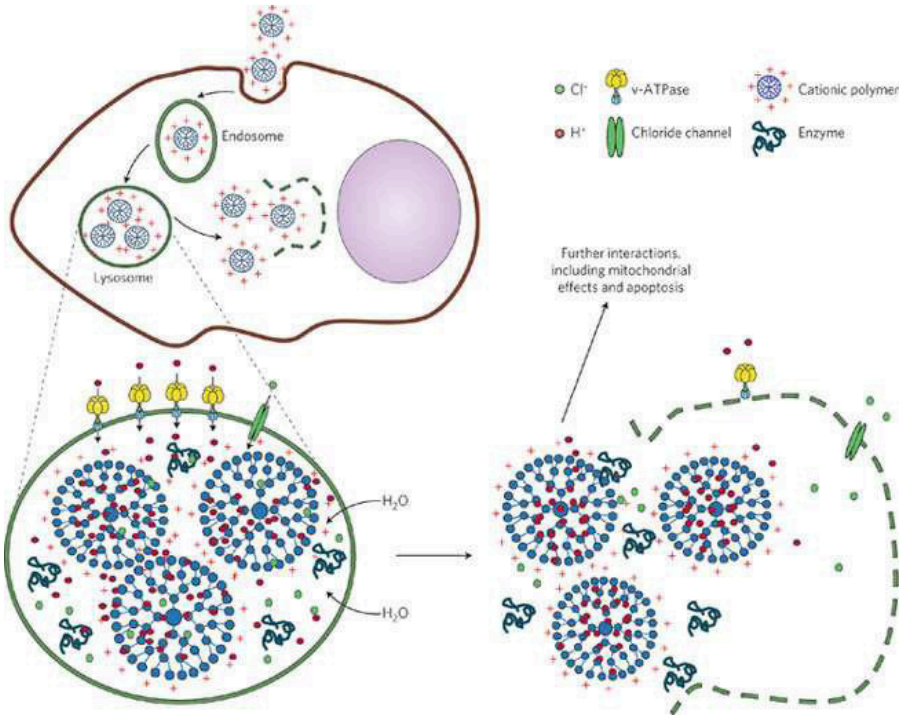

Figure 4. Proton sponge effect.Cationic particles bind with high affinity to lipid groups on the surface membrane and are endocytosed in the tight-fitting vesicles. Once these cationic nanoparticles enter into an acidifying lysosomal compartment, the unsaturated amino groups are capable of sequestering protons that are supplied by the v-ATPase (proton pump). This process keeps the pump functioning and leads to the retention of one Cl^- ion and one water molecule per proton. Subsequent lysosomal swelling and rupture leads to particle deposition in the cytoplasm and the spillage of the lysosomal content.

2.1.4 Genotoxicity

Action of toxicants in the nucleus is usually linked to genotoxicity. Direct action of NP on the sugar-phosphate backbone, for instance depurination, oxidation, methylation, formation of adducts of bases that can subsequently cause single strand breaks, can either be repaired or lead to apoptosis. Nearby single strand breaks (SSBs), SSB duplication, in-strand crosslink can lead to double strand breaks (DSBs) and chromosome breaks, which cannot be repaired. In addition, inhibition of repair enzymes may also cause an increased rate of genotoxic events, while protein lesions and abnormalities of the mitotic spindle are causes for chromosome loss[37].

Many NP smaller than 50 nm can get into the nucleus, but localization in the nucleus is not a prerequisite for action on the DNA; intracellular NP can also gain access to the genetic material during mitosis when the nuclear membrane breaks down and genotoxic changes may also be caused by interference with the mitotic spindle. Furthermore, exposition to NP lead to epigenetic changes include modifications of DNA and histones and influence the transcription rate of genes. Histone acetylation and DNA methylation are key processes in cell differentiation and transformation. It has been reported that NP can cause epigenetic changes by modulation of DNA methyltransferase activity, decreased mRNA expression of methyl-CpG-binding domain protein expression, decrease of histone deacetylase activity and histone 3 hyperacetylation[38]. ROS are involved in DNA hypomethylation and expression of methylation DNA-regulated genes. Epigenetic changes by direct effects of NP include formation of histone aggregates through interaction with quantum dots and binding of Au NP to SH-groups in histone deacetylase. Although not a direct consequence of DNA damage, NP may inhibit translation, either by hindering the export of mRNA through enlarged NP-loaded lysosomes, or by reduced expression of ribosome subunit S2[39].

3.Nanoparticles cell membrane crossing

Cell membrane helps organisms to maintain homeostasis by controlling what substances may enter or leave cell, it is composed of phospholipids, proteins and carbohydrates arranged in a fluid mosaic structure. Some substances as oxygen, carbon dioxide and water can cross the cell membrane without any input of energy by the cell, the movement of such substances across the membrane is known as passive transport. Conversely, for the passage of large and charged molecules, as proteins and sugar, energy use from ATP is required.

3.1. Passive transport

The most simply way to cross the cell membrane is the passive diffusion.
Diffusion includes the movement of molecules from an area of high concentration to one of low concentration (simple diffusion), this mechanisms can be supported for large molecule as glucose, by the presence of specific transportes on the cell membrane that allow the passage of substances (facilitate diffusion).
Osmosis is the spontaneous movement of water across the cell membrane trough the aquaporins and it is important for cell homeostasis.

3.2. Active transport

Active transport is an energy dependent pathway that allows charge and large substances to overcome cell membrane, independently from their gradient concentration.
Endocytosis is the process that occurs by the invagination of the plasmatic membrane in order to form vesicles which transport the material from outside to inside the cell. The endocytosis is divided into: endocytosis mediated by clathrin, endocytosis mediated by caveolin, macropynocytosis and phagocytosis (Figure 2.2). The endocytosis mediated by clathrin is the process by which the cells introduce nutrients and regulatory molecules. This process is highly selective and it starts with the recognition among the molecules to introduce with specific receptors which are present on the plasmatic membrane, followed by the accumulation of complex receptors-ligands in specific points of the membrane, called clathrin coated vesicles. The formation of the endocytic vesicle coated by clathrin is mediated by cytoskeletal elements of actin. Once formed, vesicles lose the clathrin coat with the formation of an uncoated vesicle, which will blend later with an endosome in order to form early endosome.

The endocytosis mediated by caveolin is the process that involved the caveolae, invaginations of the plasmatic membrane, present in several cellular types but particularly abundant in endothelial cells[40]. Caveolae are involved in the internalization of components of the plasmatic membrane, of the extracellular ligand and bacterial toxins, are formed in correspondence with regions of the plasmatic membrane which are rich in cholesterol and sphingolipids and are specially coated by caveolin, a dimeric protein, which links the cholesterol by introducing itself in the plasmatic membrane. The endocytosis is mediated by dynamin and by microfilaments of actin. One formed, caveolae pour their own material in caveosomi, which are different from endosome both for the pH and for the enzymatic content. From caveosomi the endocytosed material is distributed through transporting vesicles, to the Golgi or to the RER, where it is modified by enzymes that it contains [40]. Macropynocytosis occurs in several cellular types, as for instance the macrophages, it starts with the formations of extended protrusions of the plasmatic membrane, supported by cytoskeletal elements of actin. The protrusions blend with the same membrane to form big endocytic vesicles containing extracellular material[40]. Phagocytosis is the process by which microorganisms, cellular debris and apoptotic cells are destroyed and represents the mechanism with which protozoa are nourished. In more complex organism, phagocytosis is mainly a defensive mechanism and it is carried out by specialized cells such as macrophages, neutrophils and dendritic cells[40]. The transcytosis, instead, is a vesicular transport used by multicellular organism in order to transport in a selective way macromolecules between two compartments delimited by a polarized cell, for example the transport of the macromolecules made by endothelial cells from tissue to blood and vice versa .

This process have the same step of the endocytosis mediated by clathrin, they blend with particular apical endosomes (or basolateral), that transfer material to recycling endosome basolateral (or apical). These blend with the

basolateral (or apical) membrane, and pour the macromolecules in the opposing basolateral (or apical) side[40].

3.3. Nanoparticles cellular uptake mechanisms

Plasma membrane acts as a portal of entry to NP. Depending on NP physico-chemical properties, this entry can take place by passive diffusion without persistent membrane damage, or by disruption of plasma membrane integrity. Holes in the plasma membrane smaller than 1 μm in diameter can be sealed, and, for this reason, NP can overcome the plasma membrane passively without causing cell damage. Membrane disruption with subsequent re-sealing has, for instance, been reported for cellular entry of 14 nm SiO_2 particles[41]. Carboxylated polystyrene particles appear to generate plasma membrane discontinuities in a similar order of magnitude as 0.1% Triton ×100 [42]. NP can be uptaken by cells also via energy-dependent mechanism by two major mechanisms: phagocytosis and pinocytosis[43]. Phagocytosis occurs for particles larger than 0.5 μ m in a limited number of mammalian cell types such as macrophages and monocytes. Pinocytosis is a far more general process that can be further classified into two subcategories: macropinocytosis and micropinocytosis. Macropinocytosis involves non-selective uptake of solute macromolecules of more than 0.2 μ m diameter[44], whereas micropinocytosis (clathrin-mediated, caveolae/lipid raft-mediated, and clathrin/caveolae-independent) occurs for smaller particles in all cell types[45] (Figure 5). Given the size regime of NP commonly used for therapeutic purposes (10–200 nm), NP are expected to enter cells predominantly via micropinocytosis.

Recent investigations have revealed that size, shape[46], and surface charge[47]of NP govern entry and subsequent cytosolic access of NP into living cells. For example, cationic NP have better cell membrane penetration efficiency than

anionic NP and are shown to enter mammalian cells via a different pinocytic mechanism[48]. Likewise, particles with diameters of < 200 nm were uptaken via clathrin-coated pits, whereas caveolae-mediated internalization became predominant with increasing particle size. In addition to size and charge, NP surface functionality also plays an important role in terms of cellular uptake and eliciting cellular responses[49].However, it is not clear how changes on the NP surface (e.g. hydrophobicity and aromaticity) affect cellular internalization process.

4. Bioengineering nanoparticles to avoid endo-lysosomal pathway

To avoid NP endocitosys and hence lysosomal accumulation, some strategies have been developed. The most of them consider the modification of NP surface by using chemical or biological moieties to allow cell membrane passive diffusion or lysosomal escape.

However the modification of NP surface affects the nano-bio interface making much more complex the elucidation of the interactions between NP and biological systems.

A way to avoid NP endo-lysosomal compartement is the surface functionalization with bioactive peptides, such as cell-penetrating peptide (CPPs). CPPs are a group of relatively short peptide (5–40 amino acids) deriving either from natural sources or from synthetically designed constructs, are able to penetrate cell membranes and transport a large variety of molecule inside cells [8]. Thanks to their features as amphipathic nature, net positive charge, theoretical hydrophobicity and helical moment, CPPs are able to slip through the lipid cell membrane. CPPs enter cells presumably by means of their cationic groups initially interacting with negative charged residues of cell membrane, leaving their hydrophobic reagions free to access the membrane's hydrophobic interior.

Recently, great attention has been devoted to the study of hydrophobic peptides that efficiently traverse biological membranes, promoting lipid membrane reorganizing processes, such as fusion or pore formation and thus involving temporary membrane destabilization and subsequent reorganization[50].

Moreover, there are controversies regarding the mechanism of action when CPPs are bound on NP surface, more studies are necessary to explain their crossing membrane mechanisms.

References

1. Wim H. De Jong, Paul JA Borm. *Drug delivery and nanoparticles: applications and hazards.* International Journal of Nanomedicine, 133-149 (2008)
2. M. Ellin Doyle, 2006. *Nanotechnology: A Brief Literature Review*. Food Research Institute, University of Wisconsin–Madison.
3. Mansoori, G. Ali, and TA Fauzi Soelaiman. "Nanotechnology—an introduction for the standards community." *Journal of ASTM International* 2.6 (2005): 1-21.
4. Windler, L., et al. "Release of titanium dioxide from textiles during washing." *Environmental science & technology* 46.15 (2012): 8181-8188.
5. Silva, Gabriel A. "Nanotechnology applications and approaches for neuroregeneration and drug delivery to the central nervous system." *Annals of the New York Academy of Sciences* 1199.1 (2010): 221-230.
6. Myrtill Simkó, Ulrich Fiedeler, André Gazsó, Michael Nentwich, 2010. *Can nanoparticles end up in the brain?* Institute of Technology Assessment (ITA); Strohgasse 45/5, A-1030 Vienna.
7. Abbott, N. Joan, and Ignacio A. Romero. "Transporting therapeutics across the blood-brain barrier." Molecular medicine today 2.3 (1996): 106-113.
8. Praveen Ballabh, Alex Brown, Maiken Needergard. "The blood-barrier: an overview Structure regulation and clinical implications" Neurobiological disease (2004): 1-13
9. Wim H. De Jong, Paul JA Borm, "*Drug delivery and nanoparticles: applications and hazards".* International Journal of Nanomedicine, 133-149. (2008)
10. Misra, A., Ganesh, S., Shahiwala, A., & Shah, S. P. "Drug delivery to the central nervous system: a review". *J Pharm Pharm Sci*, *6*(2), 252-273.(2003).
11. Nevozhay D, Kañska U, Budzyñska R, Boratyñski J: "Current status of research on conjugates and related drug delivery systems in the treatment of cancer and other diseases" (Polish). Postepy HigMed Dosw, 61, 350–360 (2007)
12. Sanvicens, Nuria, and M. Pilar Marco. "Multifunctional nanoparticles–properties and prospects for their use in human medicine." *Trends in biotechnology* 26. 425-433. 8 (2008)

13. Soppimath, Kumaresh S., "Biodegradable polymeric nanoparticles as drug delivery devices." *Journal of controlled release* 70.1: 1-20. (2001)
14. Gajewicz, Agnieszka. "Advancing risk assessment of engineered nanomaterials: application of computational approaches." *Advanced drug delivery reviews* 64.15 (2012): 1663-1693.
15. Nel, A. E., Mädler, L., Velegol, D., Xia, T., Hoek, E. M., Somasundaran, P., Thompson, M. Understanding biophysicochemical interactions at the nano–bio interface. *Nature materials*, *8*(7), 543-557. (2009).
16. Verma, A., Uzun, O., Hu, Y., Hu, Y., Han, H. S., Watson, N., ... & Stellacci, FSurface-structure-regulated cell-membrane penetration by monolayer-protected nanoparticles. *Nature materials*, *7*(7), 588-595. (2008).
17. Monopoli, M. P., Åberg, C., Salvati, A., & Dawson, K. A. "Biomolecular coronas provide the biological identity of nanosized materials". *Nature nanotechnology*, *7*(12), 779-786. 2012).
18. Monopoli, M. P., Walczyk, D., Campbell, A., Elia, G., Lynch, I., Baldelli Bombelli, F., & Dawson, K. A. (2011). Physical− chemical aspects of protein corona: relevance to in vitro and in vivo biological impacts of nanoparticles. *Journal of the American Chemical Society*, *133*(8), 2525-2534.
19. Sharma, V., Shukla, R. K., Saxena, N., Parmar, D., Das, M., & Dhawan, A. (2009). DNA damaging potential of zinc oxide nanoparticles in human epidermal cells. *Toxicology letters*, *185*(3), 211-218.
20. Dewez, D., & Oukarroum, A. (2012). Silver nanoparticles toxicity effect on photosystem II photochemistry of the green alga Chlamydomonas reinhardtii treated in light and dark conditions. *Toxicological & Environmental Chemistry*, *94*(8), 1536-1546.
21. Xia, T., Kovochich, M., Brant, J., Hotze, M., Sempf, J., Oberley, T., ... & Nel, A. E. Comparison of the abilities of ambient and manufactured nanoparticles to induce cellular toxicity according to an oxidative stress paradigm. *Nano letters*, *6*(8), 1794-1807.
22. Bhattacharya, K., Davoren, M., Boertz, J., Schins, R. P., Hoffmann, E., & Dopp, E. Titanium dioxide nanoparticles induce oxidative stress and DNA-adduct formation but not DNA-breakage in human lung cells. *Part Fibre Toxicol*, *6*, 17. (2006).

23. Fröhlich, E. Cellular Targets and Mechanisms in the Cytotoxic Action of Non-biodegradable Engineered Nanoparticles. *Current drug metabolism*, *14*(9), 976. (2013)
24. Yao, Y., Qin, J., Cai, Y., Wei, F., Lu, F., & Wang, S. Facile synthesis of magnetic ZnFe2O4–reduced graphene oxide hybrid and its photo-Fenton-like behavior under visible iradiation. *Environmental Science and Pollution Research*, 1-11. (2014)
25. Lovrić, J., Cho, S. J., Winnik, F. M., & Maysinger, D. Unmodified cadmium telluride quantum dots induce reactive oxygen species formation leading to multiple organelle damage and cell death. *Chemistry & biology*, *12*(11), 1227-1234. (2005).
26. Lai, J. C., Ananthakrishnan, G., Jandhyam, S., Dukhande, V. V., Bhushan, A., Gokhale, M., ... & Leung, S. W. Treatment of human astrocytoma U87 cells with silicon dioxide nanoparticles lowers their survival and alters their expression of mitochondrial and cell signaling proteins. *International journal of nanomedicine*, *5*, 715.(2010)
27. Kao, Y. Y., Chen, Y. C., Cheng, T. J., Chiung, Y. M., & Liu, P. S Zinc oxide nanoparticles interfere with zinc ion homeostasis to cause cytotoxicity. *Toxicological Sciences*, *125*(2), 462-472.(2012)
28. Xia, Tian, et al. "Comparison of the mechanism of toxicity of zinc oxide and cerium oxide nanoparticles based on dissolution and oxidative stress properties." *ACS nano* 2.10 (2008): 2121-2134.
29. Tupling, R., & Green, H. “Silver ions induce Ca2+ release from the SR in vitro by acting on the Ca2+ release channel and the Ca2+ pump.” *Journal of Applied Physiology*, *92*(4), 1603-1610. (2002)
30. Lieu, P. T., Heiskala, M., Peterson, P. A., & Yang, Y. The roles of iron in health and disease. *Molecular aspects of medicine*, *22*(1), 1-87.(2001)
31. Chithrani, B. D., & Chan, W. C. Elucidating the mechanism of cellular uptake and removal of protein-coated gold nanoparticles of different sizes and shapes. *Nano letters*, *7*(6), 1542-1550.(2007)
32. Cho, W. S., Duffin, R., Howie, S. E., Scotton, C. J., Wallace, W. A., MacNee, W., ... & Donaldson, K. Progressive severe lung injury by zinc oxide nanoparticles; the role of Zn2+ dissolution inside lysosomes. *Part Fibre Toxicol*, *8*(1), 27.(2011)

33. Jin, C. Y., Zhu, B. S., Wang, X. F., & Lu, Q. H. Cytotoxicity of titanium dioxide nanoparticles in mouse fibroblast cells. *Chemical research in toxicology*, *21*(9), 1871-1877.(2008)

34. Funnell, W. R., & Maysinger, D. Three-dimensional reconstruction of cell nuclei, internalized quantum dots and sites of lipid peroxidation. *Journal of nanobiotechnology*, *4*(10).(2006)

35. Lundqvist, M., Stigler, J., Elia, G., Lynch, I., Cedervall, T., & Dawson, K. A.. Nanoparticle size and surface properties determine the protein corona with possible implications for biological impacts. *Proceedings of the National Academy of Sciences*, *105*(38), 14265-14270.(2008)

36. Colilla, M., González, B., & Vallet-Regí, M. Mesoporous silica nanoparticles for the design of smart delivery nanodevices. *Biomaterials Science*, *1*(2), 114-134.(2013)

37. Kim, H. R., Kim, M. J., Lee, S. Y., Oh, S. M., & Chung, K. H. Genotoxic effects of silver nanoparticles stimulated by oxidative stress in human normal bronchial epithelial (BEAS-2B) cells. *Mutation Research/Genetic Toxicology and Environmental Mutagenesis*, *726*(2), 129-135.(2011)

38. Jennifer, M., & Maciej, W. Nanoparticle Technology as a Double-Edged Sword: Cytotoxic, Genotoxic and Epigenetic Effects on Living Cells. *Journal of Biomaterials & Nanobiotechnology*, *4*(1).(2013)

39. AshaRani, P. V., Low Kah Mun, G., Hande, M. P., & Valiyaveettil, S. Cytotoxicity and genotoxicity of silver nanoparticles in human cells. *ACS nano*, *3*(2), 279-290.(2008)

40. Alberts - Johnson - Lewis – AAVV, 2009. *Biologia molecolare della cellula*. Editore, Zanichelli.

41. Mu, Q., Hondow, N. S., Krzemiński, L., Brown, A. P., Jeuken, L. J., & Routledge, M. N. Mechanism of cellular uptake of genotoxic silica nanoparticles. *Part Fibre Toxicol*, *9*(1), 29.(2012)

42. Smith, P. J., Giroud, M., Wiggins, H. L., Gower, F., Thorley, J. A., Stolpe, B., ... & Rappoport, J. Z. Cellular entry of nanoparticles via serum sensitive clathrin-mediated endocytosis, and plasma membrane permeabilization. *Int J Nanomedicine*, *7*, 2045-2055.(2012)

43. Conner, S. D., & Schmid, S. L. Regulated portals of entry into the cell. *Nature*, *422*(6927), 37-44. (2003)

44. Swanson, J. A., & Watts, C. Macropinocytosis. *Trends in cell biology*, *5*(11), 424-428. (1995).

45. Kumari, S., Swetha, M. G., & Mayor, S. Endocytosis unplugged: multiple ways to enter the cell. *Cell research*, *20*(3), 256-275.(2010).

46. Chithrani, B. D., Ghazani, A. A., & Chan, W. C. Determining the size and shape dependence of gold nanoparticle uptake into mammalian cells. *Nano letters*, *6*(4), 662-668.(2006)

47. Chen, J., Yang, M., Zhang, Q., Cho, E. C., Cobley, C. M., Kim, C., ... & Xia, Y. Gold nanocages: a novel class of multifunctional nanomaterials for theranostic applications. *Advanced Functional Materials*, *20*(21), 3684-3694.(2010)

48. Dausend, J., Musyanovych, A., Dass, M., Walther, P., Schrezenmeier, H., Landfester, K., & Mailänder, V. Uptake mechanism of oppositely charged fluorescent nanoparticles in HeLa cells. *Macromolecular bioscience*, *8*(12), 1135-1143.(2008)

49. Chompoosor, A., Saha, K., Ghosh, P. S., Macarthy, D. J., Miranda, O. R., Zhu, Z. J., ... & Rotello, V. M. The role of surface functionality on acute cytotoxicity, ROS generation and DNA damage by cationic gold nanoparticles. *Small*, *6*(20), 2246-2249. (2010)

50. G. Vitiello, A. Falanga, M. Galdiero, D. Marsh, S. Galdiero and G. D'Errico. *Biochim. Biophys.* Acta 1808, 2517.(2010)

AIM OF THE THESIS

The physico-chemical properties of nanoparticles (NP) such as, small size, possibility to being functionalized with ligands, ability to transport cargo and the potential capacity to access isolated parts of the body including brain, create a coherent interest to develop NP for therapeutic and diagnostic field. For these reasons, in order to explore their potential use, it is necessary to understand the interactions of NP with the cell membrane and their trafficking through the cells. In fact, despite numerous efforts to establish a structure–function relationship between NP physico-chemical properties and their interactions with biological systems, the possibility to predict their fate remains still far.

The aim of this thesis was to elucidate the role of nano-bio interface in controlling NP-cell interaction and, hence, cell membrane crossing mechanisms and NP cytotoxic effect.

To address this issue, we first studied the effect of NP delivery across cell membrane in controlling metal-containing NP (MNP) toxicity. In particular, we delivered MNP across the cell membrane directly inside the cytosol by using a pneumatic method -a gene gun - thus bypassing the formation of endocytic vesicles and comparing the cytotoxic effect related to different route of entry of NP.

Furthermore, we designed surface decorated NP by using a bio-inspired approach in order to control NP entrance and to escape the lysosomal pathway. We investigated the effect of the decoration of polystyrene NP with Herpes simplex virus type one derived gH-625 peptide, on intracellular trafficking and on the ability to overcome a blood-brain barrier *in vitro* model.

2. CHAPTER I

TRANSPORT ACROSS CELL-MEMBRANE DICTATES NANOPARTICLE FATE AND TOXICITY: A NEW PARADIGM IN NANOTOXICOLOGY

2.1. ABSTRACT

The toxicity of metallic nanoparticles (MNP) has been fully ascertained, but the mechanisms underlying their cytotoxicity remain still largely unclear. Here we demonstrate that the cytotoxicity of MNP is strictly reliant upon the pathway of cellular internalization. In particular, if otherwise toxic gold, silver, and iron oxide NP are forced through the cell membrane bypassing any form of active mechanism (e.g., endocytosis), no significant cytotoxic effect is registered. Pneumatically driven NP across the cell membrane show a different distribution within the cytosol compared to NP entering the cell by active endocytosis. Specifically, they exhibit free random Brownian motions within the cytosol and do not accumulate in lysosomes. Results suggest that intracellular accumulation of metallic nanoparticles into endo-lysosomal compartments is the leading cause of nanotoxicity, due to consequent nanoparticle degradation and *in-situ* release of metal ions.

2.2. Introduction

A growing body of evidence suggests that a wide variety of metal-containing nanoparticles are toxic both *in vitro* [1-4] and *in vivo* [2-3,5-8]. Among others, gold, silver and iron oxide NP have been reported as toxic for several cell types, such as cancer cells [1], neuroendocrine cells [9], germline stem cells [10],

macrophages [11] and human umbilical vein endothelial cells [12]. Furthermore, *in vivo* tests have evidenced that exposure to metallic nanoparticles (MNP) causes dysfunctions of the intestinal apparatus in embryonic Zebrafish models [13], defects in the embryonic development of Xenopus laevis [14], phenotypic modifications in the progeny of Drosophila melanogaster [6,15], as well as decrease in body weight, red blood cells, hematocrit and DNA damage in mice[16-17]. These studies have shown that the production of reactive oxygen species (ROS), genotoxicity and apoptosis are a common consequence of exposure to MNP[18-26]. Nevertheless, little is known about the mechanisms underlying the interaction of MNP with biological systems and the actual cause of toxicity. It appears that amongst the various pathways/targets involved in MNP' toxicity, mitochondrial damage and metallic ion production are relevant factors. However, it is not known whether the cellular damage is a consequence of metallic ion production, ROS production or a particle-related effect [5,26].

In this framework, despite repeated attempts to establish a structure–function relationship between their physico-chemical properties and their interactions with biological systems, the possibility to predict the toxicological profile of nanoparticles is still far away.

In order to better understand the mechanisms of MNP' cytotoxicity, it is helpful to look at organelles, where accumulation is most likely. In most of the studies, MNP are allowed to enter the cell through the canonic endocytic pathways and appear to be stored in lysosomes upon incubation with cells [27-31]. Accumulation within the degradative lysosomal compartment might cause MNP' cytotoxicity; however, no direct evidence of this effect has been reported yet, due to the difficulty to bypass the endo-lysosomal pathway. In this work, we postulated that the cell entrance pathway dictates NP' intracellular localization and, as a consequence, their toxic potential. The idea is that the cytotoxicity of MNP does not depend on the physico-chemical features of the MNP *per se*, but rather on the microenvironmental conditions

they experience during their journey towards the intracellular space that, in turn, depend upon how they cross the cell membrane. To test this hypothesis, we delivered MNP across the cell membrane directly inside the cytosol by using a pneumatic method – a gene gun - thus bypassing the formation of endocytic vesicles. Gene guns are popular as a means of incorporating DNA or RNA into cells; they use micro- and nano-particles as bullets fired into cells and tissues using pressurized gas[32-34]. Here we used a gene gun to deliver different metal-containing NP, namely 40 nm Au NP, 20 nm Ag NP and 25 nm silica-coated Fe_3O_4 NP, known to be cytotoxic for several cell types and *in vivo* [1,9,12 35-36], to a mouse brain endothelial bEnd.3 and human cervical adenocarcinoma HeLa cell lines. To assess the effects of the internalization mechanism on nanoparticles' cytotoxicity, the same nanoparticles were delivered by "classical" endocytosis upon incubation to the same cell lines. The physico-chemical characterization of the NP is reported in Table 1. Moreover, 44 and 100 nm fluorescent polystyrene (PS) NP (Table 1) were used, respectively, as a negative control in cytotoxicity studies [37] and for multiple particle tracking (MPT) and confocal laser scanning microscopy (CLSM) analyses. The intracellular behavior of the NP, the cell viability
and the ROS generation were analyzed in order to find a correlation among the internalization pathways, the intracellular localization and the cell response.

2.3. Results

2.3.1. NP intracellular trafficking and localization

To evaluate the effects of the internalization mechanism on NP' localization and behavior within the cytosol, we analyzed in detail the mechanisms of intracellular motion at high frequencies of 100 nm fluorescent amine-

modified PS NP by a multiple particle tracking (MPT) technique. We have previously demonstrated that, when exposed to the cell surfaces, 100 nm PS NP are uptaken by endothelial cells through endocytic mechanisms and tend to accumulate in lysosomes[38-39]. Similarly, in this work we observed that, incubating PS NP with cells, most of the NP are internalized by endocytosis and show a pearl-on-a-string behavior, characteristic of vesicular transport (Fig. 1 a and b). Only a small fraction of the NP followed a random walk movement within the cytosol (Fig. 1 a and c). On the other hand, the same NP forced through the cell membrane by pneumatic-shooting showed almost exclusively random walk trajectories, indicating that most of the NP were not encapsulated inside endocytic vesicles (Fig. 1 a and c). To further confirm the different intracellular localization of shot *vs.* endocytosed (endo) NP, we performed indirect inmmunofluorescence analysis against the lysosomal marker LAMP2. Endo NP clearly showed a significant co-localization with lysosomes (Fig. 1 d), while no co-localization was observed for shot NP (Fig. 1 e).

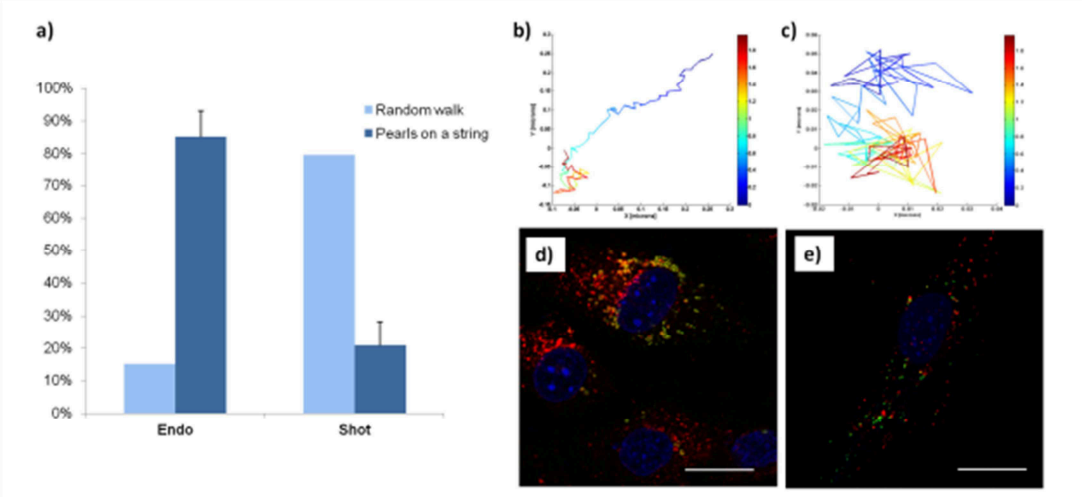

Figure 1. MPT analysis of endo and shot 100 nm PS NP in bEnd.3 cells. a) Percentage of "random walk" and "pearls on a string" trajectories as a function of internalization mechanism. Representative examples of (b) "pearls on a string" and (c) "random walk" trajectories. Confocal images showing the co-localization (yellow) of (d) endo and (e) shot 100 nm PS NP (green) with lysosomes (red). Magnification bar 20 µm.

Starting from MPT and confocal microscopy observations with fluorescent PS NP, the intracellular localization of endo and shot Au NP was also investigated by TEM analysis. Fig. 2 demonstrates the presence of Au NP inside the cells. In particular, endo Au NP were confined in vesicular structures (typically organized as aggregates), presumably multivesicular bodies (MVBs), and no free particles in the cytosol were observed (Fig. 2 a). These results confirmed the data reported in literature demonstrating the accumulation of endo Au NP within vesicular structures of the endo-lysosomal pathway in different cell lines[40-41]. Conversely, most of shot NP were freely dispersed in the cytoplasm (Fig. 2 b), and only a few NP aggregates were observed.

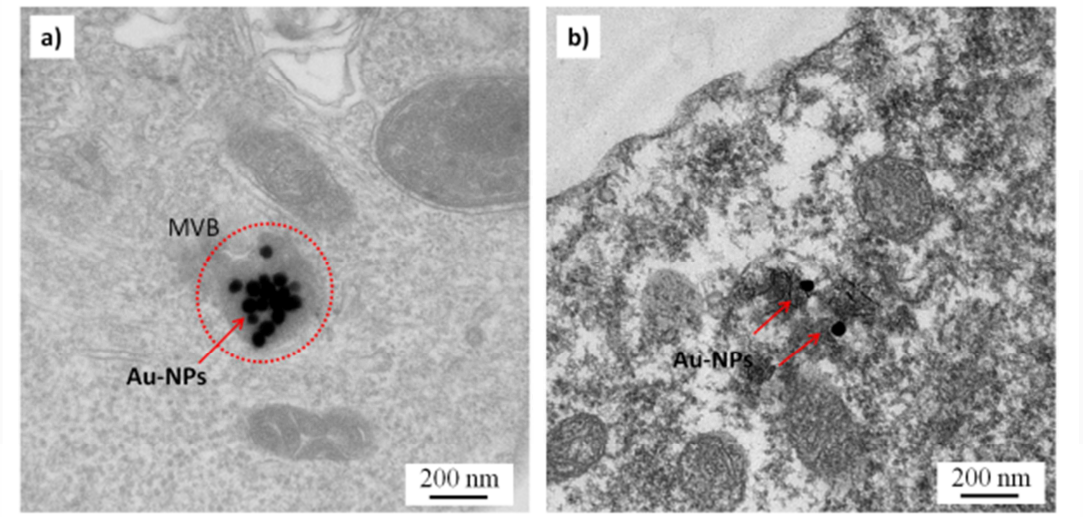

Figure 2. Intracellular localization of (a) endo and (b) shot Au NP in bEnd.3 cells by TEM analysis. Endo Au NP were confined in vesicular structures, presumably multivesicular bodies (MVBs), and no free particles in the cytosol were observed. Shot NP were observed to be free in the cytosol.

TEM observations were in agreement with the co-localization analysis of 100 nm PS NP with lysosomes. Altogether, these results demonstrated the main accumulation of endo Au NP in vesicular structures, as opposed to the homogeneous distribution of shot Au NP in the cytosol. The above validates the hypothesis that the way NP are transported through the membrane strongly affects their cytosolic distribution, and that the passive passage

across the cell membrane - pushing the NP by pneumatic forces - avoids their endo-lysosomal compartment localization.

2.3.2. Cytotoxicity

The different intracellular distribution of shot and endo MNP could lead to a different impact of NP on cell functions. To address this hypothesis, cell viability and ROS generation upon Au, Ag and Fe_3O_4 NP' exposure were investigated. In these experiments, we compared the cytotoxic effects of endocytosed *vs.* shot NP, normalizing the effective dose of internalized NP obtained with the two procedures, through ICP measurements (Supplementary Fig. 1 and 3).

The cytotoxicity of endo and shot NP on bEnd.3 and HeLa cells was first evaluated by Alamar blue assay. Experimental results show that MNP were significantly cytotoxic when endocytosed by bEnd.3 cells (Fig. 3). In particular, Ag NP were more cytotoxic than Au and Fe_3O_4 NP, already at lower concentrations. Moreover, a large decrease in cell viability was observed after 5 days of culture. Conversely, by comparing the same doses of shot NP per cell, no cytotoxic effects were detected for any MNP. Interestingly, at the highest concentrations, endo Ag NP led to a drastic decrease in cell viability (> 80%) already after 24 h incubation, unlike shot Ag NP. No cytotoxic effects were observed for both shot and endo 44 nm negatively charged PS NP used as a negative control (Supplementary Fig. 3). Similar results were obtained also for the HeLa cell line after exposure to Au and Fe_3O_4 NP (Fig. 4 and Supplementary Fig. 4), thus further validating our observations.

As mentioned above, one of the main causes of MNP' cytotoxicity is oxidative stress. Therefore, we investigated the effect of NP' endocytosis and shooting on ROS generation levels in bEnd.3 cells through DCF assay.

Figure 5 shows that ROS generation increased for endo NP at the highest concentrations. Moreover, the effect of Ag and Fe_3O_4 NP on ROS generation was more evident than that of Au NP. Conversely, shot NP did not significantly augment intracellular ROS levels. Only a slight, non-statistically significant increment of ROS generation was observed for Ag and Fe_3O_4 NP. Taken altogether, the above results indicate that the endo MNP are significantly more toxic than shot MNP and that is more relevant considering that endo MNP are covered by protein corona which is known to reduce nanoparticles' cytotoxicity[37,42-43].

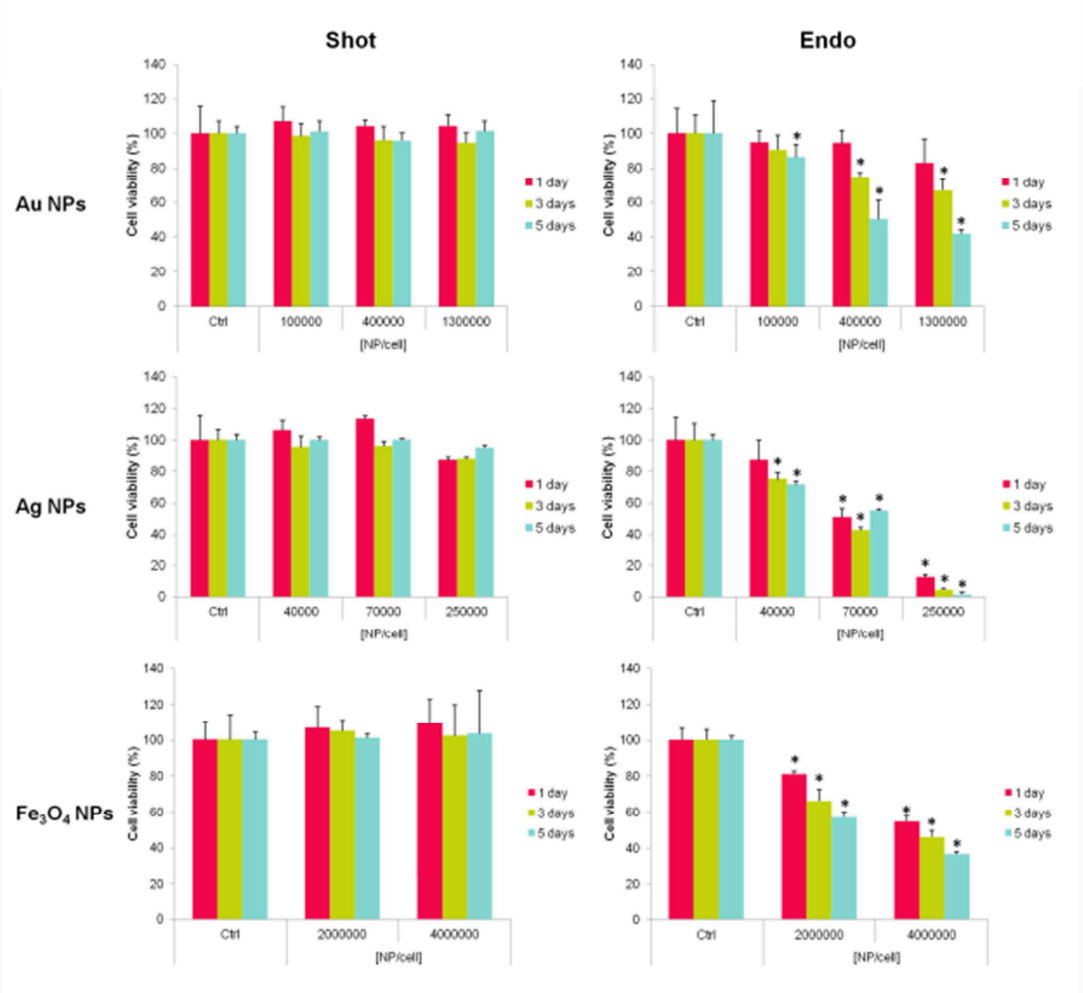

Figure 3. *In vitro* cytotoxicity by Alamar blue assay of Au NP, Ag NP and Fe_3O_4 NP. Data were reported as percentage of cell viability normalized to cells treated with 44 nm negatively charged PS NP, used as negative control, at 4×10^5 NP/cell concentration. Error bars indicate the standard deviation. *$p < 0.05$ compared to control (n= 9).

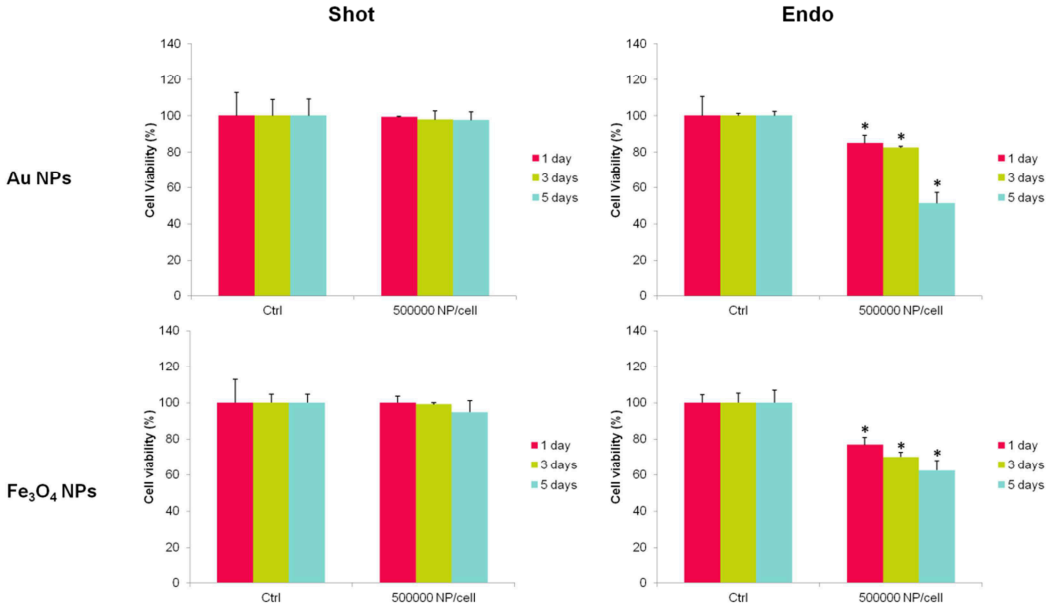

Figure 4. *In vitro* cytotoxicity by Alamar blue assay of shot and endo Au and Fe_3O_4 NP incubated 24 h with HeLa cells at the concentration of 5×10^5 NP/cell. Data were reported as percentage of cell viability normalized to control cells. Error bars indicate the standard deviation. *$p < 0.05$ compared to control (n= 9).

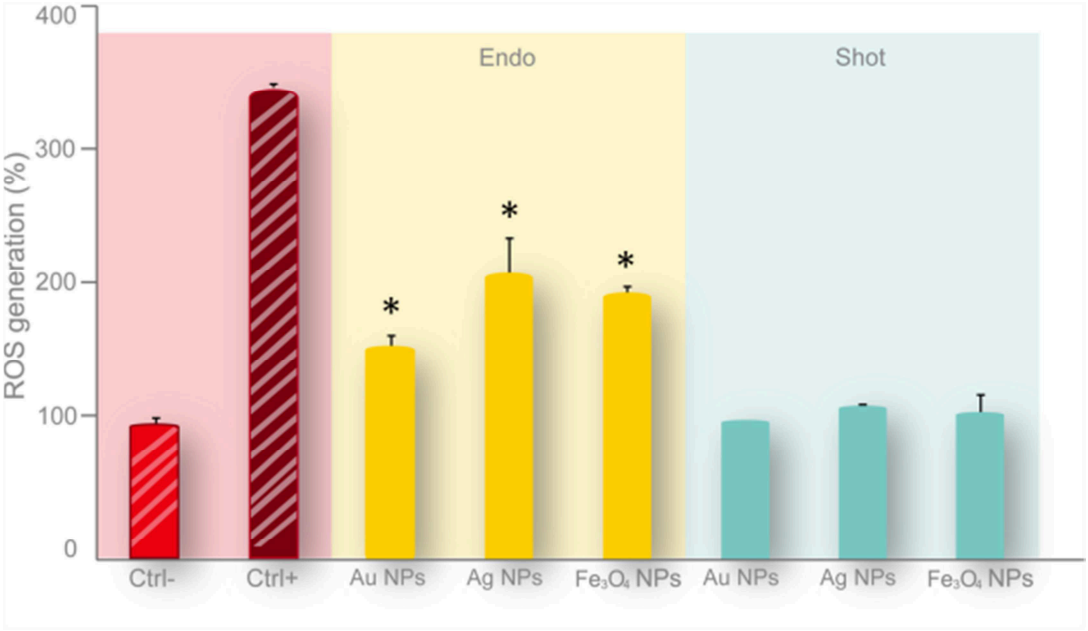

Figure 5. Effects of MNP' endocytosis and shooting on the level of ROS in bEnd.3 cell line, probed by the DCFH-DA assay. Cells were treated with the highest NP concentrations, corresponding to 1.3×10^6 Au NP/cell, 2.5×10^5 Ag NP/cell and 4.0×10^6 Fe_3O_4 NP/cell, respectively. The ROS level of nanoparticle-treated cells was expressed with respect to non-treated control cells (Ctrl -). As a positive control (Ctrl +), cells were incubated with 100 µM H_2O_2. Error bars indicate the standard deviation. *$p < 0.05$ compared to negative control (n= 9).

2.4. Discussion

Our data indicate that the different mechanism of internalization affects the interaction of NP with cells. A possible explanation of this effect could rely on intracellular release of metal ions. In fact, when in the lysosomal compartments, NP are subjected to lower pH levels and an overall degradative environment. Indeed, recent works reported on the effect of pH on MNP' degradation and -consequently- ion release, not only in buffers but also in cells [36,44-46]. Therefore, we hypothesized that NP' degradation and consequent intracellular release of metallic ions, is the main cause of MNP' toxicity upon endocytosis. We observed an increase in metallothionenis (MTs) expression in HeLa cells upon exposure to 0.6 nM endo Ag NP compared to shot NP and non-treated control cells (data not shown). MTs are major cytoplasmic metal ions binding proteins and thereby reduce cellular damage caused by toxic heavy metals, including Ag [47-49]. Also, some recent works reported MTs' up-regulation associated with MNP' toxicity [50]. Moreover, we observed that Ag NP toxicity can be significantly prevented by treatment with specific ion chelators. For instance, both cell viability and ROS levels in HeLa cells were found to be similar to the control levels following treatment with the chelating agent meso-2,3-Dimercaptosuccinic acid (DMSA). However, further investigation is needed to elucidate the detailed molecular mechanisms underlying MNP' toxicological effects after cellular internalization. In summary, this study demonstrates the correlation between MNP' intracellular localization, MNP' fate and cytotoxicity. In particular, our data clearly indicate that - by changing MNP' uptake mechanism and, therefore, MNP' intracellular localization - it is possible to modify MNP' behavior and their impact on cell functions. These findings are of particular interest for nanomedicine and nanotoxicology, and pave the way to new and appealing questions about mechanisms underlying MNP' toxicity. Moreover, our results demonstrate the validity of the ballistic method to

circumvent endo-lysosomal pathways. Although such technique uses an un-natural way to cross cell-membrane, this study offers the opportunity to investigate the interaction of MNP with cytosolic structures thus finding new targets for novel MNP' biological effects and possible applications. Furthermore, it suggests some guidelines to consider for the rational design of safer MNP. In particular, the engineering of the MNP' surface to avoid lysosomal degradation or its functionalization with specific molecules able to escape lysosomal fate[30,38] could be valid strategies in order to obtain non-toxic MNP.

2.5. Materials and methods

2.5.1. Materials

Orange fluorescent amine-modified polystyrene, 100 nm, nanoparticles (100 PS NP) were purchased by Sigma-Aldrich. Green fluorescent polystyrene, 44 nm, nanoparticles (44 PS NP) were purchased by Duke Scientific Corporation. Au NP, Ag NP and silica-coated iron oxide (Fe_3O_4) NP were purchased from HiQ-Nano.

2.5.2. Characterization of nanoparticles

Measurements of size and ζ-potential of NP were made with a Zetasizer Nano-ZS (Malvern Instruments, Worcestershire, UK) and by a transmission electron microscope (TEM Tecnai G^2, Fei).

2.5.3. Cell culture

Immortalized mouse cerebral endothelial cells, bEnd.3 cells (American Type Culture Collection, Manassas, VA) were grown in DMEM with 4.5 g/L glucose, 10% Fetal Bovine Serum (FBS), 3.7 g/L sodium bicarbonate, and 4 mM glutamine, 1% non-essential amino acids, 100 U/ml penicillin and 0.1 mg/ml streptomycin in 100 mm diameter cell culture dish, in a humidified atmosphere at 37°C and 5% CO_2. Cells used in all experiments were at passage 11–18. Human epithelioid cervix carcinoma, HeLa cells (American Type Culture Collection, Manassas, VA) were maintained with DMEM with 4.5 g/L glucose, 10% Fetal Bovine Serum (FBS), 3.7 g/L sodium bicarbonate, and 4 mM glutamine, 1% non-essential amino acids, 100 U/ml penicillin and 0.1 mg/ml streptomycin at 37°C and 5% CO_2.

2.5.4. Endocytic NP uptake experiments

To allow NP uptake through endocytosis process, about 3×10^4 cells were incubated with NP suspensions in cell culture medium at different concentrations, 0.05, 0.1, 0.5, 1 and 2 nM, for 24h at 37 °C. After incubation, cells were rinsed with PBS to remove non-internalized NP and fresh culture medium was added.

2.5.5. NP intracellular shooting by ballistic system

To have NP free in the cytoplasm, a ballistic system (gene gun, BioRad) was used according to the manufacturer's procedure. Briefly, 30 µl of MNP suspension in absolute ethanol at different concentrations (2, 4, 6 and 8 nM) were deposited and left to dry on a rupture disk under a sterile hood. On the other hand, 44 and 100 nm PS NP were suspended in 30 µl of distilled water

at the final concentration of 4.2×10^{13} and 9.2×10^{12} NP/ml, respectively, deposited and left to dry on a rupture disk under a sterile hood. After solvent drying, a 900 psi pressure was used to shoot NP within cells. After shooting, cells were roughly rinsed with PBS to remove non-internalized NP and, the day after, the cells were recovered and 3×10^4 cells were seeded in each fresh 35 mm culture dish.

2.5.6. Multiple particle tracking

Images of shot and endo 100 nm PS NP in End3 cells were collected in time-lapse for about 100 s with a sampling time of 1 s by using a widefield fluorescence microscope (Olympus Cell-R, 60x oil immersion objective, NA = 1.35). Tracking algorithm has been described in details elsewhere [39]. NP' trajectories were built and then the mean square displacement (MSD) was calculated and correlated with the NP' diffusion by the equation (1),

$$MSD = 4Dt^{\alpha}$$

where D is the diffusion coefficient and α represents the time dependence. By fitting the MSD curve of each tracked bead by using equation (1), information concerning the nature of particle motion into the cells was gained. Nanoparticles, exhibiting MSD curve that undergoes a power law with exponent minor or equal to unity, were classified as Brownian ($\alpha=1$) or sub-diffusive ($\alpha<1$). Particles presenting MSD, whose dependence on time was well described by the power law with $\alpha>1$, were indicated as super-diffusive. In particular, about the α coefficient we can distinguish three critical cases: $\alpha = 0$, for immobile NP (displacement does not change with time); $\alpha = 1$, for a randomly moving NP; $\alpha = 2$ for NP moving in a straight line at a constant velocity. For $1<\alpha < 2$ an overlap between random and straight motion is found, reflecting the NP' active motion along the filaments due to the action of molecular motors. The percentages of randomly moving NP ($\alpha \leq 1$) and transported NP ($1<\alpha < 2$) were evaluated and compared for

shooting and endocytosis. The MSD of 216 and 226 distinct objects for endo and shot NP samples, respectively, was evaluated. For each experiment, at least, 5 cells were analyzed.

2.5.7. Colocalization with lysosomes

For co-localization experiments, after 100 nm PS NP' incubation, cells were firstly rinsed twice with PBS to remove non-internalized nanoparticles and fixed with 4% paraformaldehyde for 20 min. Then, cells were incubated with Triton X100 0.1% in PBS for 10 min and with PBS-BSA 0.5% for 15 min at room temperature (RT). Lysosomes were localized with rabbit anti-LAMP 2 polyclonal (Abcam) primary antibodies and with 568 goat anti-rabbit secondary antibodies (Molecular Probes, Invitrogen). All samples were then observed at confocal microscope (SP5 Leica) with a 63x oil immersion objective.

2.5.8. Transmission electron microscopy (TEM)

TEM was performed to precisely localize the intracellular nanoparticles. After gold NP' exposure, cells were rinsed with PBS and fixed with 2.5% glutaraldehyde in 0.1 M sodium cacodylate buffer for 2h at room temperature. Afterwards, cells were post-fixed with 1% osmium tetroxide in 0.1 M sodium cacodylate buffer for 1h at 4 °C, dehydrated in graded concentrations of ethanol (30%, 50%, 70%, 95% and 100%). Cell samples were then scraped, harvested and embedded in Epon (Electron Microscopy Science, EMS) and thin-sectioned with an ultramicrotome (UC7, Leica). Sections of 70 nm were collected on copper grids and stained with lead citrate and uranyl acetate. The grids were visualized by a TEM Tecnai G^2 (Fei).

2.5.9. Quantification of internalized nanoparticles

To evaluate the number of endo and shot NP within cells, after NP' incubation, cells were roughly rinsed with PBS, trypsinized and counted by Neubauer chamber. Afterward, cells were centrifuged and the pellets were lysed with lysis buffer (7 M urea, 2 M thiourea, 4% CHAPS, 30 mM Tris). Cell lysates were analyzed by a spectrofluorometer (Perkin–Elmer, USA) to measure the amount of internalized PS NP and through elemental analysis, carried out by inductively coupled plasma atomic emission spectroscopy (ICP-AES) with an Agilent 700 Series spectrometer, to evaluate the intracellular amount of Au, Ag and Fe-Si. Data were reported as NP number normalized to the number of cells. Samples that had the same number of NP per cell were used and compared each other for cytotoxicity and ROS generation analyses.

2.5.10. In vitro cytotoxicity

Cell viability was quantified by Alamar Blue Assay and compared to non-treated cells, which were used as a control. Briefly, 3×10^4 cells were seeded on a 35 mm cell culture dish and incubated 24 h with NP suspensions to allow endocytosis. Conversely, for NP' shooting, cells were shot with NP by gene gun, washed roughly with PBS and, then, allowed to recover for 24 h at 37 °C. After recovery, cells were trypsinized, counted and seeded on fresh 35 mm cell culture dishes. Alamar Blue Assay was performed according to the manufacturer's procedure at 1, 3 and 5 days after NP exposure. Absorbance of Alamar Blue reagent solution was read at 570 nm and 600 nm by a plate reader (Perkinelmer). Data were reported as percentage of viable cells normalized to non-treated cells.

2.5.11. DCFH-DA assay

bEnd.3 cells were treated with metallic NP at the highest concentrations, corresponding to 1.3×10^6 Au NP/cell, 2.5×10^5 Ag NP/cell and 4.0×10^6 Fe-Si NP/cell, respectively, and then seeded in 24- well microplates. After 24 h of culture, the DCFH-DA (20,70-dichlorofluorescein diacetate, Sigma) assay was performed. Briefly, the cells were washed with PBS buffer and then incubated with 1 mM DCFH-DA in the loading medium (DMEM 1% FBS) for 60 min at 37 °C. After the loading medium was removed, the DCFH-DA loaded cells were placed in a microplate reader (Perkin Elmer) and the fluorescence intensity was measure by setting the excitation filter at 485 nm and the emission filter at 530 nm. As a negative control, we applied the same assay onto untreated cells. Results were normalized with respect to negative controls (expressed as 100%). As a positive control for cytotoxicity, cells were incubated with 100 μM H_2O_2.

Statistical analyses. Quantitative data were reported as mean ± standard deviation (SD). Statistical analyses were performed using a one-way analysis of variance (ANOVA). Results repeats were compared by analysis of variance (ANOVA), and a p value < 0.05 was considered statistically significant

REFERENCES

1. Maiorano, G.*, et al.* Effects of Cell Culture Media on the Dynamic Formation of Protein-Nanoparticle Complexes and Influence on the Cellular Response. *Acs Nano* **4**, 7481-7491 (2010).
2. Mahmoudi, M., Azadmanesh, K., Shokrgozar, M.A., Journeay, W.S. & Laurent, S. Effect of Nanoparticles on the Cell Life Cycle. *Chemical Reviews* **111**, 3407-3432 (2011).
3. Shi, H., Magaye, R., Castranova, V. & Zhao, J. Titanium dioxide nanoparticles: a review of current toxicological data. *Particle and Fibre Toxicology* **10**(2013).
4. Yong, K.-T.*, et al.* Nanotoxicity assessment of quantum dots: from cellular to primate studies. *Chemical Society Reviews* **42**, 1236-1250 (2013).
5. Ma, H., Williams, P.L. & Diamond, S.A. Ecotoxicity of manufactured ZnO nanoparticles - A review. *Environmental Pollution* **172**, 76-85 (2013).
6. Vecchio, G.*, et al.* Mutagenic effects of gold nanoparticles induce aberrant phenotypes in Drosophila melanogaster. *Nanomedicine-Nanotechnology Biology and Medicine* **8**, 1-7 (2012).
7. Sabella, S.*, et al.* Toxicity of citrate-capped AuNP: an in vitro and in vivo assessment. *Journal of Nanoparticle Research* **13**, 6821-6835 (2011).
8. Brunetti, V.*, et al.* InP/ZnS as a safer alternative to CdSe/ZnS core/shell quantum dots: in vitro and in vivo toxicity assessment. *Nanoscale* **5**, 307-317 (2013).
9. Kim, T.-H.*, et al.* Size-dependent cellular toxicity of silver nanoparticles. *Journal of Biomedical Materials Research Part A* **100A**, 1033-1043 (2012).
10. Braydich-Stolle, L., Hussain, S., Schlager, J.J. & Hofmann, M.C. In vitro cytotoxicity of nanoparticles in mammalian germline stem cells. *Toxicological Sciences* **88**, 412-419 (2005).
11. Stroh, A.*, et al.* Iron oxide particles for molecular magnetic resonance imaging cause transient oxidative stress in rat macrophages. *Free Radical Biology and Medicine* **36**, 976-984 (2004).

12. Wu, X., Tan, Y., Mao, H. & Zhang, M. Toxic effects of iron oxide nanoparticles on human umbilical vein endothelial cells. *International Journal of Nanomedicine* **5**, 385-399 (2010).
13. Özel, R.E., Alkasir, R.S.J., Ray, K., Wallace, K.N. & Andreescu, S. Comparative Evaluation of Intestinal Nitric Oxide in Embryonic Zebrafish Exposed to Metal Oxide Nanoparticles. *Small*, n/a-n/a (2013).
14. Bacchetta, R.*, et al.* Nano-sized CuO, TiO2 and ZnO affect Xenopus laevis development. *Nanotoxicology* **6**, 381-398 (2012).
15. Vecchio, G.*, et al.* Concentration-Dependent, Size-Independent Toxicity of Citrate Capped AuNP in Drosophila melanogaster. *Plos One* **7**(2012).
16. Zhang, X.-D.*, et al.* Toxicologic effects of gold nanoparticles in vivo by different administration routes. *International Journal of Nanomedicine* **5**, 771 (2010).
17. Shukla, R.K., Kumar, A., Vallabani, N.V.S., Pandey, A.K. & Dhawan, A. Titanium dioxide nanoparticle-induced oxidative stress triggers DNA damage and hepatic injury in mice. *Nanomedicine*, 1-11 (2013).
18. Johnston, H.J.*, et al.* Identification of the mechanisms that drive the toxicity of TiO2 particulates: the contribution of physicochemical characteristics. *Particle and Fibre Toxicology* **6**(2009).
19. Pan, Y.*, et al.* Gold Nanoparticles of Diameter 1.4 nm Trigger Necrosis by Oxidative Stress and Mitochondrial Damage. *Small* **5**, 2067-2076 (2009).
20. Heng, B.C.*, et al.* Evaluation of the cytotoxic and inflammatory potential of differentially shaped zinc oxide nanoparticles. *Archives of Toxicology* **85**, 1517-1528 (2011).
21. Xu, H.*, et al.* Role of reactive oxygen species in the antibacterial mechanism of silver nanoparticles on Escherichia coli O157:H7. *Biometals* **25**, 45-53 (2012).
22. Suliman Y, A.O.*, et al.* Evaluation of cytotoxic, oxidative stress, proinflammatory and genotoxic effect of silver nanoparticles in human lung epithelial cells. *Environmental Toxicology*, n/a-n/a (2013).
23. Ye, Y.*, et al.* Nano-SiO2 induces apoptosis via activation of p53 and Bax mediated by oxidative stress in human hepatic cell line. *Toxicology in Vitro* **24**, 751-758 (2010).

24. Naqvi, S.*, et al.* Concentration-dependent toxicity of iron oxide nanoparticles mediated by increased oxidative stress. *International Journal of Nanomedicine* **5**, 983-989 (2010).
25. Srivastava, R.K.*, et al.* Multi-walled carbon nanotubes induce oxidative stress and apoptosis in human lung cancer cell line-A549. *Nanotoxicology* **5**, 195-207 (2011).
26. Kim, S. & Ryu, D.-Y. Silver nanoparticle-induced oxidative stress, genotoxicity and apoptosis in cultured cells and animal tissues. *Journal of Applied Toxicology* **33**, 78-89 (2013).
27. Chithrani, B.D., Ghazani, A.A. & Chan, W.C.W. Determining the size and shape dependence of gold nanoparticle uptake into mammalian cells. *Nano Letters* **6**, 662-668 (2006).
28. Faklaris, O.*, et al.* Photoluminescent Diamond Nanoparticles for Cell Labeling: Study of the Uptake Mechanism in Mammalian Cells. *Acs Nano* **3**, 3955-3962 (2009).
29. Goya, G.F.*, et al.* Dendritic cell uptake of iron-based magnetic nanoparticles. *Cell Biology International* **32**, 1001-1005 (2008).
30. Nativo, P., Prior, I.A. & Brust, M. Uptake and intracellular fate of surface-modified gold nanoparticles. *Acs Nano* **2**, 1639-1644 (2008).
31. Rejman, J., Oberle, V., Zuhorn, I.S. & Hoekstra, D. Size-dependent internalization of particles via the pathways of clathrin-and caveolae-mediated endocytosis. *Biochemical Journal* **377**, 159-169 (2004).
32. Klein, T.M., Wolf, E.D., Wu, R. & Sanford, J.C. HIGH-VELOCITY MICROPROJECTILES FOR DELIVERING NUCLEIC-ACIDS INTO LIVING CELLS. *Nature* **327**, 70-73 (1987).
33. Klein, R.M., Wolf, E.D., Wu, R. & Sanford, J.C. High-velocity microprojectiles for delivering nucleic acids into living cells. 1987. *Biotechnology (Reading, Mass.)* **24**, 384-386 (1992).
34. Abdelrahim, M., Safe, S., Baker, C. & Abudayyeh, A. RNAi and cancer: Implications and applications. *Journal of RNAi and gene silencing : an international journal of RNA and gene targeting research* **2**, 136-145 (2006).
35. Pompa, P.P.*, et al.* Physical assessment of toxicology at nanoscale: nano dose-metrics and toxicity factor. *Nanoscale* **3**, 2889-2897 (2011).

36. Malvindi, M.A., *et al.* Toxicity Assessment of Silica Coated Iron Oxide Nanoparticles and Biocompatibility Improvement by Surface Engineering. *Plos One* **9**, e85835 (2014).
37. Wang, F., *et al.* The biomolecular corona is retained during nanoparticle uptake and protects the cells from the damage induced by cationic nanoparticles until degraded in the lysosomes. *Nanomedicine-Nanotechnology Biology and Medicine* **9**, 1159-1168 (2013).
38. Guarnieri, D., *et al.* Shuttle-Mediated Nanoparticle Delivery to the Blood-Brain Barrier. *Small* **9**, 853-862 (2013).
39. Guarnieri, D., Guaccio, A., Fusco, S. & Netti, P.A. Effect of serum proteins on polystyrene nanoparticle uptake and intracellular trafficking in endothelial cells. *Journal of Nanoparticle Research* **13**, 4295-4309 (2011).
40. Chithrani, B.D., Stewart, J., Allen, C. & Jaffray, D.A. Intracellular uptake, transport, and processing of nanostructures in cancer cells. *Nanomedicine-Nanotechnology Biology and Medicine* **5**, 118-127 (2009).
41. Ma, X., *et al.* Gold Nanoparticles Induce Autophagosome Accumulation through Size-Dependent Nanoparticle Uptake and Lysosome Impairment. *Acs Nano* **5**, 8629-8639 (2011).
42. Lesniak, A., *et al.* Effects of the Presence or Absence of a Protein Corona on Silica Nanoparticle Uptake and Impact on Cells. *Acs Nano* **6**, 5845-5857 (2012).
43. Kim, J.A., *et al.* Correction to Low Dose of Amino-Modified Nanoparticles Induces Cell Cycle Arrest. *Acs Nano* (2013).
44. Singh, R.P. & Ramarao, P. Cellular uptake, intracellular trafficking and cytotoxicity of silver nanoparticles. *Toxicology Letters* **213**, 249-259 (2012).
45. Soenen, S.J., *et al.* The effect of nanoparticle degradation on poly(methacrylic acid)-coated quantum dot toxicity: The importance of particle functionality assessment in toxicology. *Acta Biomaterialia*.
46. Galeone, A., *et al.* In vivo assessment of CdSe-ZnS quantum dots: coating dependent bioaccumulation and genotoxicity. *Nanoscale* **4**, 6401-6407 (2012).
47. Nath, R., Kambadur, R., Gulati, S., Paliwal, V.K. & Sharma, M. MOLECULAR ASPECTS, PHYSIOLOGICAL-FUNCTION, AND CLINICAL-SIGNIFICANCE

OF METALLOTHIONEINS. *Crc Critical Reviews in Food Science and Nutrition* **27**, 41-85 (1988).

48. Kooncumchoo, P., Sharma, S., Porter, J., Govitrapong, P. & Ebadi, M. Coenzyme Q(10) provides neuroprotection in iron-induced apoptosis in dopaminergic neurons. *Journal of Molecular Neuroscience* **28**, 125-141 (2006).
49. Sharma, S., Rais, A., Sandhu, R., Nel, W. & Ebadi, M. Clinical significance of metallothioneins in cell therapy and nanomedicine. *International Journal of Nanomedicine* **8**, 1477-1488 (2013).
50. Hohnholt, M.*, et al.* Handling of Iron Oxide and Silver Nanoparticles by Astrocytes. *Neurochem Res* **38**, 227-239 (2013).

Supporting information

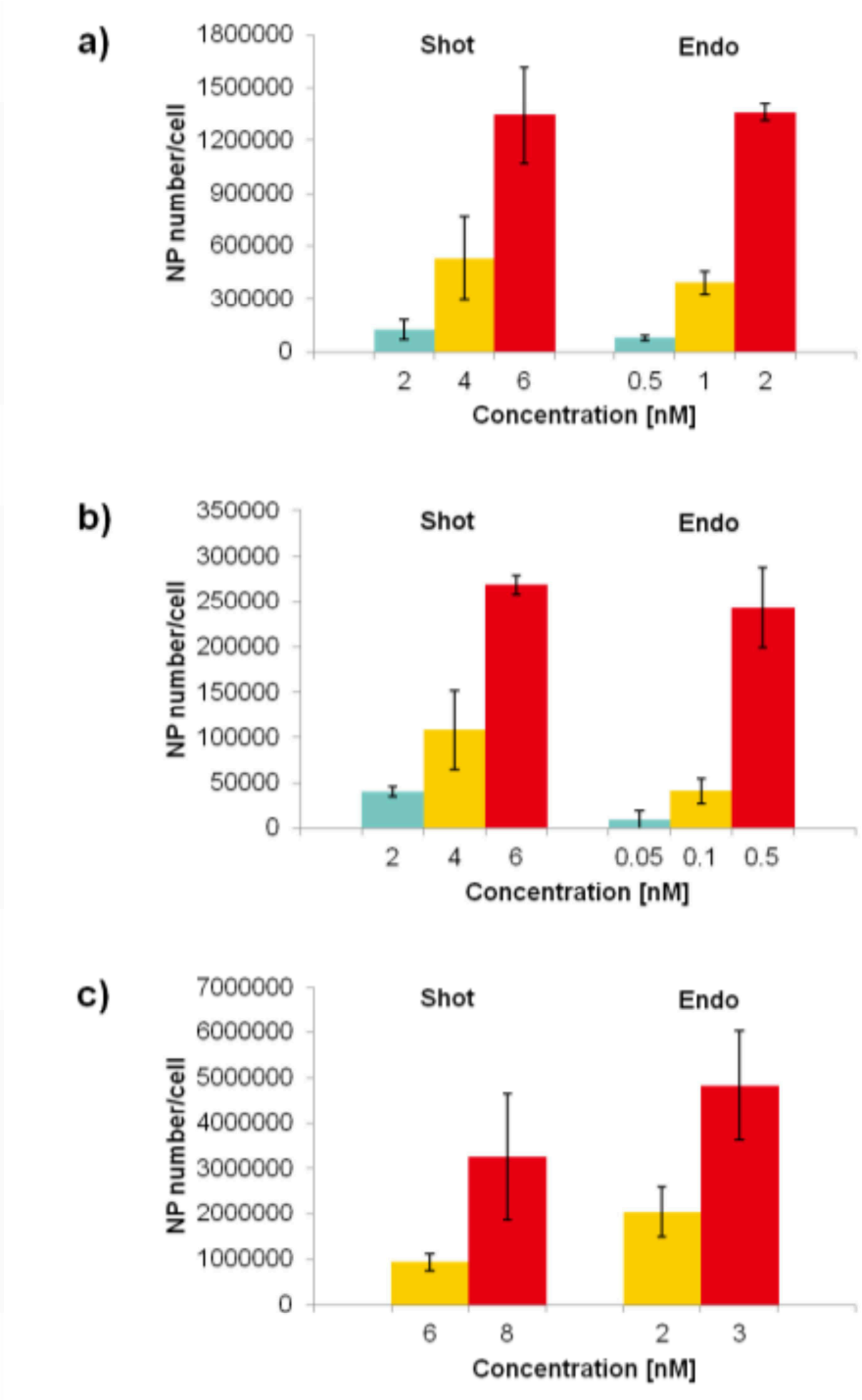

Figure S1. Quantification of internalized endo and shot NP through ICP elemental analysis after 24 h incubation in bEnd.3 cells. Au NP (a), Ag NP (b) and Fe3O4 NP (c). Data were expressed as NP number/cell. Error bars indicate the standard deviation.

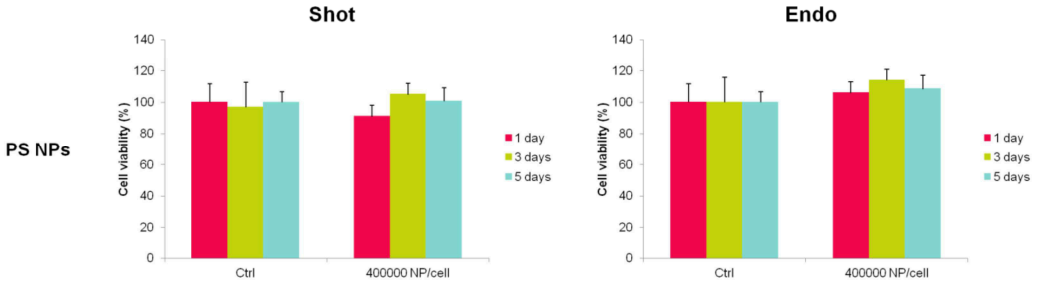

Figure S2. *In vitro* cytotoxicity by Alamar blue assay of shot and endo 44 PS NP incubated 24 h with bEnd.3 cells at the concentration of 4 × 105 NP/cell. Data were reported as percentage of cell viability normalized to control cells. Error bars indicate the standard deviation. No statistically significant differences were found between NP' treatments and controls.

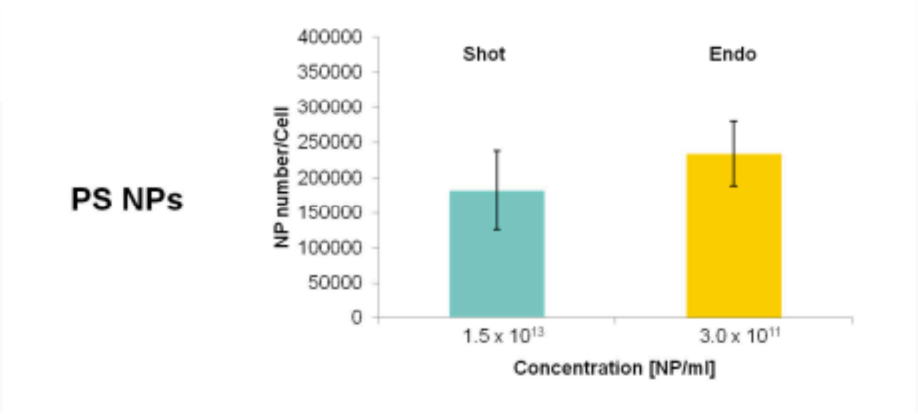

Figure S3. Quantification of internalized shot and endo 44 PS NP in HeLa cells through spectrofluorometer and ICP analysis. HeLa cells were exposed to 1.5 × 1013 PS NP/ml for shooting and 3.0 × 1011 PS NP/ml for endocytosis. Data were expressed as NP number per cell. Error bars indicate the standard deviation.

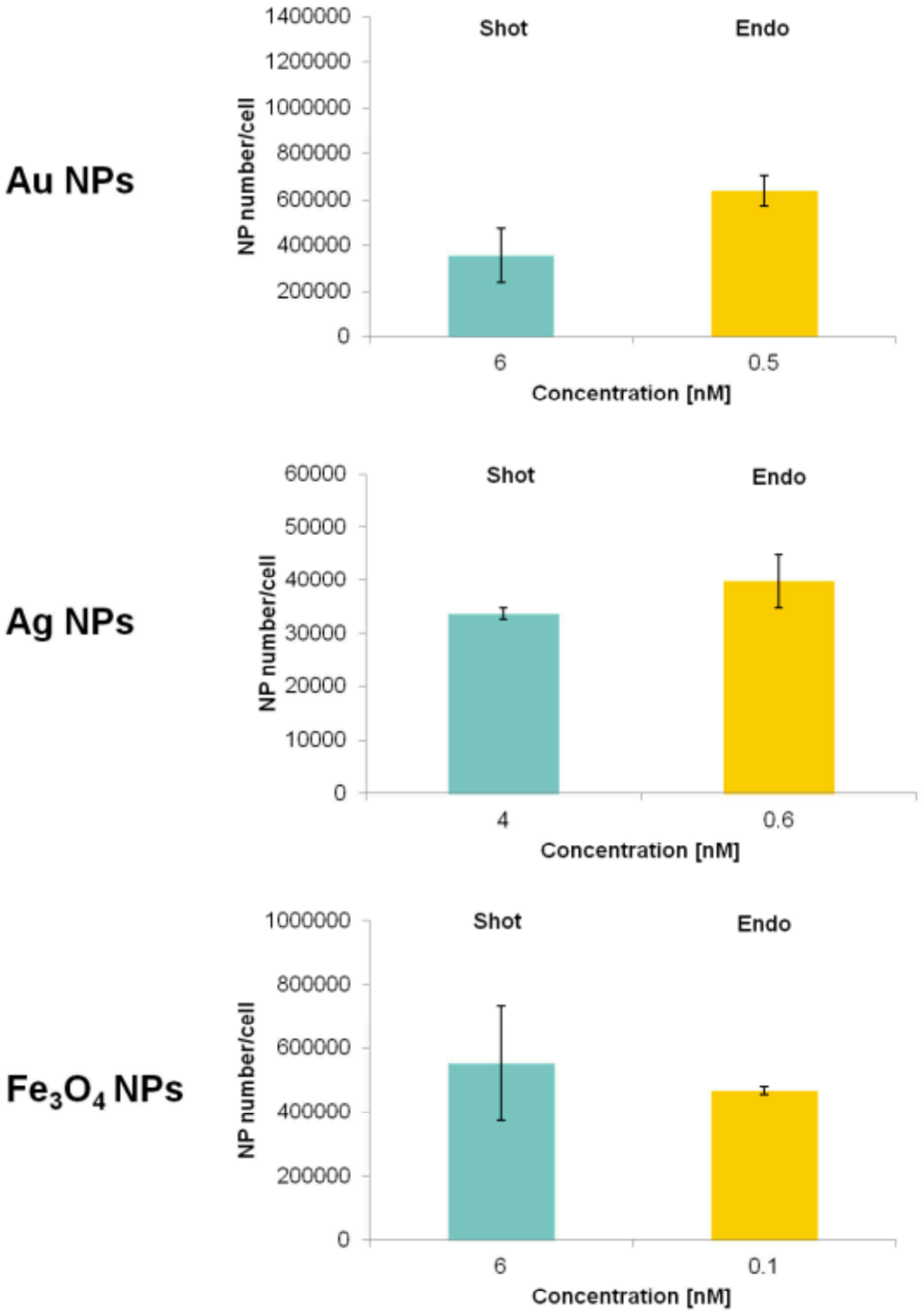

Figure S4. Quantification of internalized shot and endo Au, Ag and Fe3O4 NP in HeLa cells through spectrofluorometer and ICP analysis. For Au NP, HeLa cells were exposed to 6 nM for shooting and 0.5 nM for endocytosis. For Ag NP, HeLa cells were exposed to 4 nM for shooting and 0.6 nM for endocytosis. For Fe3O4 NP, HeLa cells were exposed to 6 nM for shooting and 0.1 nM for endocytosis. Data were expressed as NP number per cell. Error bars indicate the standard deviation.

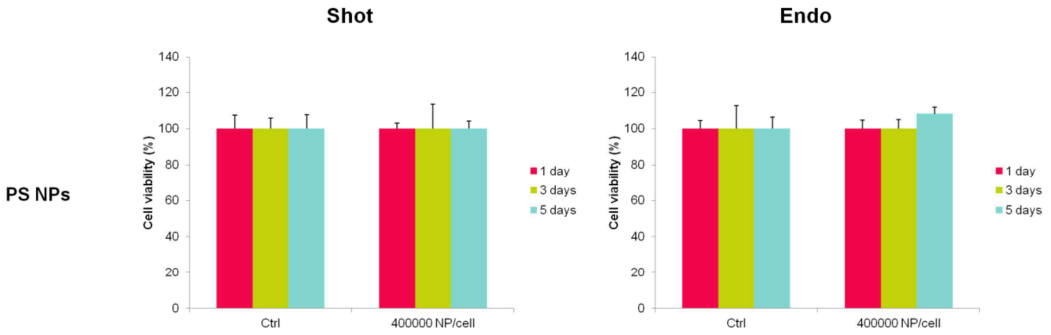

Figure S5. *In vitro* cytotoxicity by Alamar blue assay of shot and endo 44 PS NP incubated 24 h with HeLa cells at the concentration of 4 × 105 NP/cell. Data were reported as percentage of cell viability normalized to control cells. Error bars indicate the standard deviation. *$p < 0.05$ compared to control (n= 9).

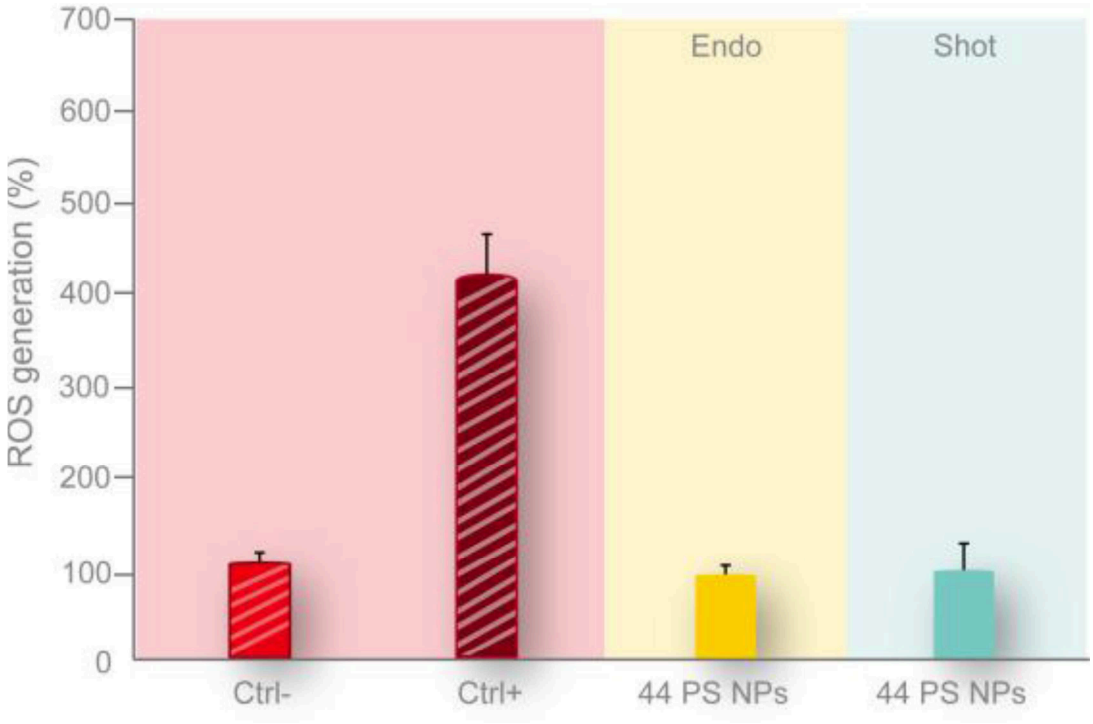

Figure S7. Effects of NP shooting (a) and endocytosis (b) on the level of ROS in bEnd.3 cell line, probed by the DCFH-DA assay. Cells were treated with 4 × 105 44 PS NP/cell. For the experiment, red fluorescent 44 PS NP were used in order to avoid interferences with green fluorescent DCF. The ROS level of nanoparticle-treated cells was expressed relative to non-treated control cells (Ctrl -). As a positive control (Ctrl +), cells were incubated with 100 µM H2O2. Error bars indicate the standard deviation. No statistically significant differences were found between NP' treatments and negative control.

Table 1. Size by TEM and DLS and ζ-potential of metallic and polystyrene nanoparticles used for experiments. DLS measurements were made at 25 °C in aqueous solutions and were repeated 5 times.

*PDI < 0.1. The TEM size of the Fe_3O_4 refers to the silica coated NP, while the value of the Fe_3O_4 core is reported in brackets (10 nm).

	Au NP	**Ag NP**	**Fe_3O_4 NP**	**44 PS NP**	**100 PS NP**
Size by TEM [nm ± SD]	40.0 ± 2.3	20.0 ± 2.1	25 ± 1.2 (10.1 ± 2.1)	41.5 ± 3.4	96.0 ± 6.7
Size by DLS [nm ± SD]*	42.9 ± 6.2	21 ± 2.0	27.2 ± 3.5	43.67 ± 0.01	102.57 ± 2.64
ζ-potential [mV ± SD]	-43.0 ± 5.0	-16 ± 2.0	-31.2 ± 5.4	-36.2 ± 6.9	+51.6 ± 1.08

3.CHAPTER II

SURFACE DECORATION AS A WAY TO ESCAPE ENDO-LYSOSOMAL COMPARTMENT AND REDUCE NANOPARTICLE TOXICITY.

3.1.ABSTRACT

Nanoparticles (NP) have access to isolated part of the body including the brain, for these reasons create great interest for biomedical applications as imaging, diagnostic and therapeutic. It is well established that the most part of NP enter the cell by endocytic pathway even if the underlying in depth mechanisms used to overcome cell membrane is not well understood. Furthermore, the fate and toxic effect of non-biodegradable NP are related to the accumulation in lysosomes. In fact, once in the lysosomes, NP can affect cell viability leading to lysosomal swelling, rupture of lysosome-endosome membrane, reactive oxygen species production, apoptosis and cell cycle arrest.

In this chapter, we provide a valid strategy to functionalize NP in order to escape endo-lysosomal pathway and, hence, avoiding NP toxic effects.

To this aim, a viral fusion peptide (gH-625) derived from the glycoprotein gH of Herpes simplex type 1 is developed, which possesses several advantages including high cell translocation potency, absence of toxicity of the peptide itself, and the feasibility as an efficient carrier for delivering therapeutics. It is hypothesized that the endo-lysosomal escape of NP conjugated with gH-625 should be efficiently obtained. The surface of fluorescent aminated polystyrene nanoparticles (NP) is functionalized with gH-625 via a covalent binding procedure, and multiple particle tracking time resolved experiment, co-localization with lysosome markers and analysis of lysosome size were performed in mouse brain endothelial cell line (bEnd3).

Data show that gH-625-NP have prevalently a “random walk” behaviour that remains almost constant in the time. Furthermore, they do not form large aggregates compared to non-functionalized NP and there is no evidence of lysosome swelling. Furthermore gH-625-NP represent the same behaviour of non-decorated NP allowed to enter the cell by avoiding endo-lysosomal pathway (gene gun). Most importantly, once bound to the surface of 50 nm positively charged NP, known for their high cytotoxic potential, there are no toxic effects.

In summary, these results suggest that surface functionalization with gH-625 may change NP cellular fate by providing a good strategy for the design of nanoparticles to the safe delivery of drugs. However, further investigation are necessary to better elucidate the mechanism by which gH-625-NP is able to avoid lysosome accumulation and, hence, to limit NP toxic effects.

3.2. Introduction

In recent years, the development of nano-sized materials in diagnostic and therapeutic field has increased in order to improve the detection and treatment of human diseases. In this direction, it is becoming necessary to better elucidate the mechanisms underlying the interactions of nanomaterials, including nanoparticles (NP), with living tissues in order to evaluate biological consequences associated with these technologies and design more effective and safe nanomaterials[1].

Physicochemical properties of NP such as surface charge, size and functionalization, play a pivotal role in controlling NP-cell interaction and many works have evidenced how these NP features can influence NP cellular uptake[2]. For instance, the propensity of the most part of NP to enter the cell through classical endocytic pathways is widely reported. The conventional picture of this mechanism involve NP binding to the plasma membrane, transport from early to late endosome, and terminal delivery to

lysosome[1,3](Figure 1). If made of not biodegradable materials, NP tend to accumulate and to remain into lysosomes, which represent their final destination.[2-3] Bio-persistence of NP has been demonstrated for iron oxide, polystyrene, gold and quantum dots; they can accumulate in lysosomes where the degradation of inorganic NP is unlikely[4]. Even if lysosome accumulation of NP occurs useful for treatment of lysosomal defects[5], it has been reported that this accumulation lead to the lysosomal impairment and swelling, reactive oxygen species (ROS) generation, cell cycle arrest and cytotoxicity[6-8]. Dawson et al. have demonstrated that, once into lysosome, polystyrene (PS) aminated 50 nm NP lose their protein corona thus exposing their bare surface material. As a consequence, this causes the rupture of lysosome and, hence, the activation of apoptosis mechanisms. These findings suggest that physico-chemical properties of NP surface can affect the intracellular journey of NP and their impact on cell viability[9].

Starting from these observations, a way to control the fate of NP could be the modification/functionalization of NP surface with molecules that reduce their degradation within the lysosomes or, alternatively, that allow NP to escape the endo-lysosomal pathway.

To address this issue, in this chapter, we report the effects of surface functionalization of 100 nm diameter amine-modified polystyrene NP with gH-625.

gH-625 is a nineteen residues fusion peptide derived from herpes simplex virus type 1 envelope, belonging to the cell penetrating peptide class (CCPs) [10]. This amphipathic peptide is characterized by net positive charge, hydrophobicity and a helical moment. Thanks to these features, the peptide is *per se* able to interact with the membrane lipids. Delivery of gH-625 peptide across cellular membrane involves several mechanisms such as direct transfer through cell surface membrane by lipid membrane fusion or transient permeabilization of the cell membrane; or after endocytosis, transfer across vesicular membranes by lipid distruption, pore formation or fusion[10-11].

However, little is known about gH-625 conjugated NP on membrane crossing mechanisms and how it affects the NP journey and their final localization inside the cells.

The aim of this study has been to better elucidate the intracellular fate of gH-625-NP and how this peptide could affect NP impact on cells by influencing endocytic pathway and intracellular trafficking.

To this aim, the cellular uptake mechanisms and the intracellular behaviour of covalently conjugated gH-625 NP was evaluated and compared to non functionalized blank-NP. Furthermore, we tested also the capability of the functionalization with gH-625 peptide to reduce the cytotoxic effect of 50 nm amine-modified PS NP, known to be cytotoxic, inhibit cell proliferation and induce lysosome impairment. Our results indicate that gH-625 peptide is able to escape lysosomal accumulation of NP and, also, suggest that the surface functionalization with this peptide could be a good strategy to design safe and effective nanoparticles, thus improving their theranostic applications.

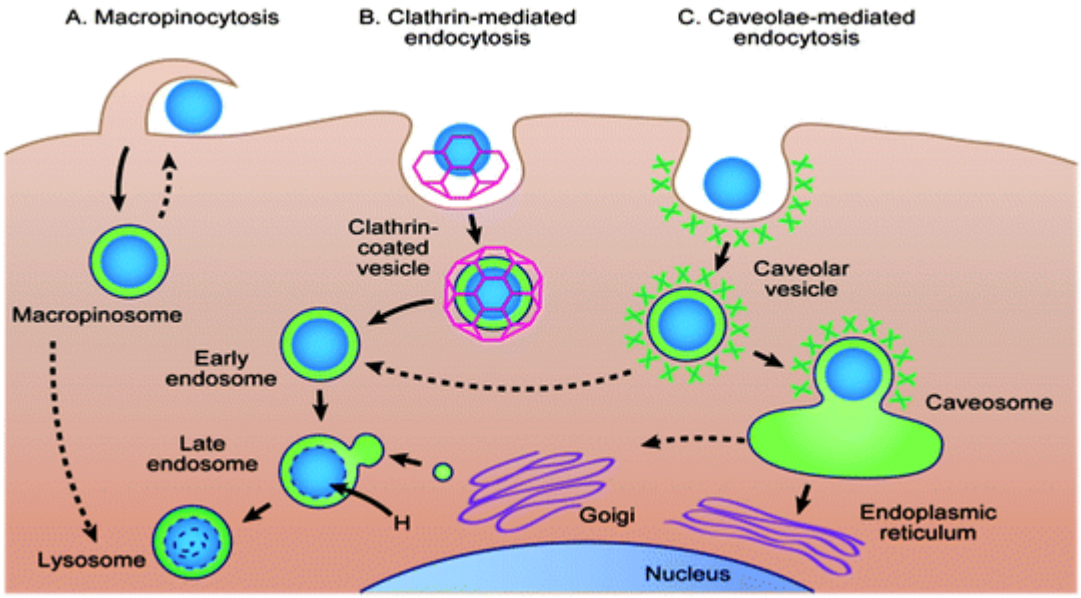

Figure 1 schematic representation of endocytic pathway (Hans -Peter Geber, Natural product reports, 2012)

3.3. Results and discussion

3.3.1. Characterization of peptide conjugated nanoparticles

To verify the secondary structure of the peptide bound to the nanoparticles we performed circular dichroism (CD) experiments. CD data confirmed that gH-625 retains its structure (helical) when bound to the nanoparticle surface as previously reported also for other peptides. The spectra obtained at different percentages of functionalization indicate a helical structure in all conditions (Figure 2 A and B).

To further investigate the effect of the peptide functionalization (25, 35 and 50%) on the size of nanoparticles, we performed dynamic light scattering (DLS) measurements. After functionalization, the hydrodynamic size of nanoparticles with 25, 35 and 50% of gH-625 in aqueous medium at pH 7 was found to be respectively 96.68 ± 0.43 nm, 95.64 ± 0.19 nm and 96.76 ± 0.07 nm, with polydispersity values of ca. 0.08, indicating a narrow distribution of the particle size at the pH used for all the experiments (Table1). To elucidate the colloidal stability of functionalized nanoparticles at different pH values, which is a crucial parameter correlated to their functionalization, measurements of the zeta potential and of the hydrodynamic radius (DH) were carried out (Table 1). For NP alone, the colloidal stability is strongly pH-dependent because it is mainly due to electrostatic repulsion between particles. It is widely accepted that at high values of z-potential (over 30 mV, positive or negative) the electrostatic interactions between particles are strong enough for electrostatic stability, while at intermediate values of z-potential, near their isoelectric point, particles can flocculate. Table 1 shows both z-potential and mean hydrodynamic diameter of blank NP and NP at different degrees of functionalization as a function of pH. In presence of peptide, the DH of the functionalized NP remained nearly constant over the entire pH range, with no

sign of aggregation in spite of the lower values of the zeta potential observed at pH 8. Such a behavior highlights that their stabilization is via steric hindrance rather than electrostatic repulsion. In particular, by increasing the percentage of functionalization NP zeta potential increases from about +30 mV to +35 mV at pH7. At these zeta potential values, NP DH remains nearly about 100 nm. Only at pH 8, we observed a lower zeta potential for 25% functionalized NP, indicating that in this condition the functionalized nanoparticles are still partially aggregated and their behaviour is similar to non-functionalized NP.

These data indicate that the peptide bound to the NP is able to retain its helical structure in all the conditions tested and is able to completely prevent NP aggregation at 35 and 50% of functionalization.

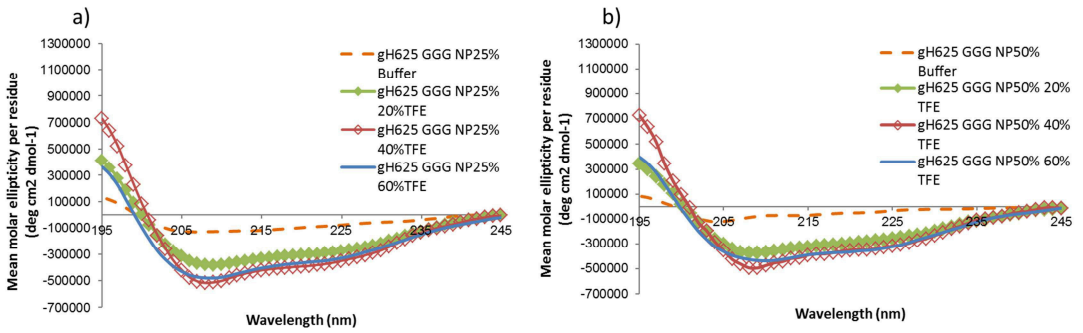

Fig.2 Circular dichroism spectra of polystyrene NP at 25% (a) and 50% (b) degrees of functionalization with gH-625

	NP		NP gH625 25%		NP gH625 35%		NP gH625 50%	
pH	Size(nm)	Z-Potential (mV)	Size(d. nm)	Z-Potential (mV)	Size(d. nm)	Z-Potential (mV)	Size(d. nm)	Z-Potential (mV)
4	137,93(±1,04)	39,97 (±0,5)	242,2(±1,49)	33,13(±1,11)	114,93(±1,4)	34,13(±2,42)	102,1(±0,36)	38,3(±1,98)
7	131,9(±0,20)	51,57(±1,08)	96,58(±0,43)	30,77(±2,40)	95,64(±1,09)	30,9(±0,79)	96,76(±0,07)	35,1(±2,43)
8	848,42(±0,60)	-11,07(±0,60)	103,37(±1,14)	10,93(±0,76)	96,27(±0,67)	18,43(±0,91)	97,53(±0,20)	17,77(±0,76)
9	473,6(±1,81)	-32(±1,22)	231,77(±6,67)	-33,33(±1,36)	99,92(±0,50)	-33,17(±1,07)	99,65(±0,70)	-28,03(±1,82)

Table1. Zeta potential and size measurements of pure NP and NP at different degrees of functionalization as a function of pH

3.3.2. Effect of gH-625 peptide conjugation on NP intracellular trafficking.

We previously demonstrated that the conjugation of the peptide gH-625 enhances cellular uptake of quantum dots[14a] and liposomes[14b] in HeLa cells *in vitro*. However, no evidences of the effect of gH-625 on nanoparticle uptake in brain endothelial cells have been previously reported. Moreover, the exact mechanism used by gH-625 to facilitate cargos transport through cell membranes has not yet been understood in details. Therefore, in this work we studied the effect of gH-625 on polystyrene NP uptake mechanisms on mouse brain endothelial bEnd3 cells.

We first tested the cytotoxicity of blank NP and gH-625-NP on bEnd3 cell line by Alamar Blue Assay and we verified that blank NP and gH-625-NP at 50% functionalization did not affect cell viability in the experimental condition used for the assay compared to non-treated control cells (data not shown).

Once internalized, NP can follow different fates: i.e. particle degradation inside lysosomal compartments, accumulation in other organelles, recycling to the plasma membrane or transcytosis to the basal surface of endothelium. Furthermore, the routes of NP intracellular trafficking might give some indications not only about the fate of NP, but also about the mechanisms driving cellular uptake.[16] To address this issue, multiple particle tracking (MPT) gives a strong contribution compared to traditional techniques (spectroscopy, microscopy, etc.)[17]. In particular, MPT technique can provide quantitative (diffusivity and velocity) and qualitative (transport mode and directionality) information of internalized NP, by evaluating the time-resolved trajectories of tens of NP. Therefore, in order to study the effect of NP surface functionalization with gH-625 on NP internalization mechanism, we followed and analyzed their intracellular motion. Figure 2 shows a snapshot of the detected trajectories generated by MPT routines. By shape,

trajectories can already be split in two different types: i) Brownian-like trajectories, suggesting NP random movement between cytosolic structures, and ii) pearls-on-a-string trajectories, derived by a combination of random and linear walk, indicative of motor protein facilitated transport, mediated by endocytic vesicles and motor proteins [18]. Evaluating the time dependence of mean square displacement (MSD) of each tracked NP we classified the particles transport mechanisms into diffusive and super-diffusive motion. In particular, to perform NP diffusive mode classification we evaluated the exponent of each fitting MSD curve by the equation described in the Methods section.

Particle trajectories revealed a substantial heterogeneity in particle intracellular dynamics, both for blank NP and gH-625-NP. However, for blank NP, most trajectories resulted in a combination of random and linear walk with a pearls-on-a-string trajectory, indicative of motor protein facilitated transport, mediated by endocytic vesicles (Figure 3). Whereas, only a lower percentage of blank NP appeared to follow a purely diffusive behavior (random walk), suggesting no particular interaction between NP and cytosolic structures (Figure 4).

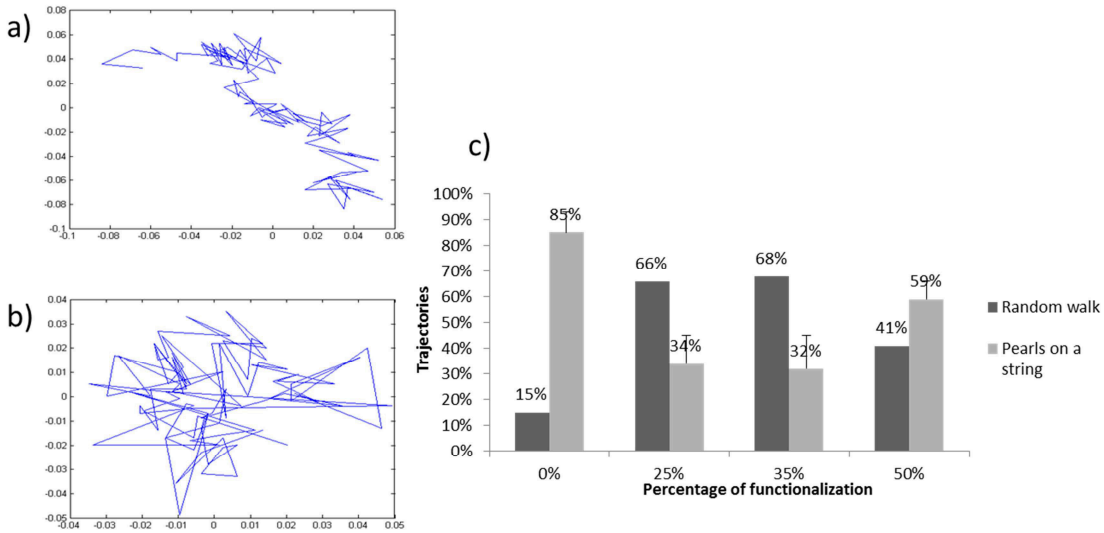

Figure 4. MPT analysis of blank and gH-625-NP. Examples of "random walk" (a) and "pearls on a string" (b) trajectories. c) Percentage of "random walk" and "pearls on a string" trajectories as a function of functionalization degree.

Conversely, in presence of peptide functionalization, we observed that most trajectories showed a random walk behaviour while a lower percentage resulted in a pearls-on-a-string trajectory. In particular, this behaviour is more evident at lower percentages of functionalization with an optimum at 35% peptide functionalization degree.

These data suggest that the effect of the peptide could depend on its concentration/density on the NP surface. In fact, we theoretically estimated the surface density of peptide of about 3, 4 and 6 peptides/nm2 for 25%, 35% and 50% functionalized NP, respectively. We hypothesized that a lower peptide surface density (3 and 4 peptides/nm2) could promote the correct peptide orientation and interaction with membrane lipids. Conversely, a higher peptide surface density (6 peptides/nm2) hinders the correct orientation of peptide aminoacidic residues and their interaction with cell membrane. Indeed, recently, we structurally characterized gH-625−644 peptide in a membrane-mimicking DPC micellar environment to gain insight into how gH fuses with the cell membrane[19]. We reported a model of gH-625 peptide structure and orientation indicating that both electrostatic and hydrophobic interactions work in concert to mediate membrane penetration. In particular, the function of the aromatic residues is to cause the peptide insertion into the membrane interface while the basic residues stabilize this interaction by linking the negatively charged headgroups as shown in other systems using both NMR[20] and EPR[21].

Since we observed that the 35% functionalized NP showed a good stability in aqueous suspension and the ability to penetrate cells using a random walk behavior, we performed all the other experiments at this percentage of functionalization.

3.3.3 Uptake mechanisms of peptide conjugated NP

Nanoparticles usually enter the cells using a cell-mediated mechanism, called endocytosis. After endocytosis, endosomes can fuse with lysosomes or can

deliver their cargo across the cell by transcytosis processes. Several works reported that caveolae are involved in the endocytosis and transcytosis processes in brain endothelial cells.Thus, in order to study if the nanoparticle functionalization with gH-625 could affect the mechanisms of NP internalization, we performed confocal microscope analyses to investigate the colocalization of NP with lysosomes and caveolae in absence of peptide and with 35% of peptide functionalization. Figure 5 shows that both blank and gH-625-NP partially colocalized with lysosomes.

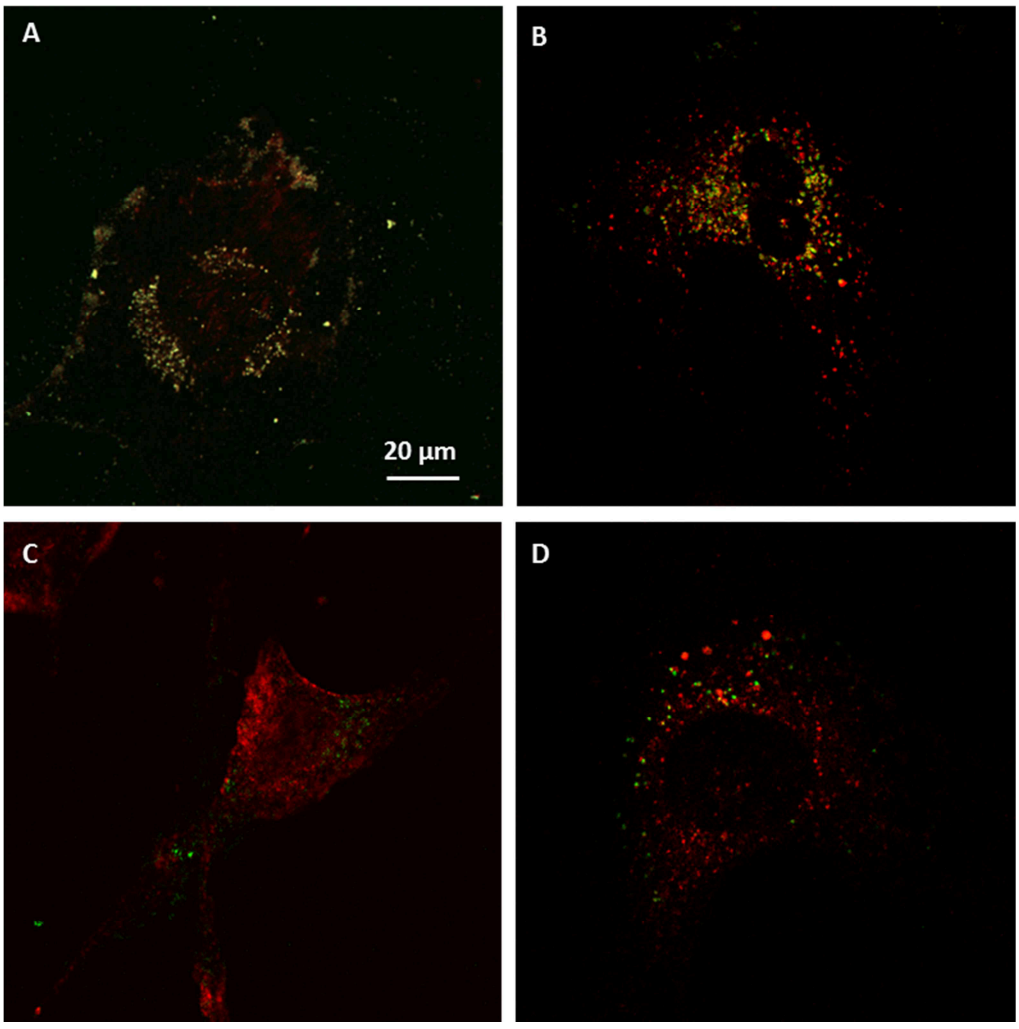

Figure 5. Colocalization of non-functionalized (a and b) and gH-625-functionalized (c and d) NP with caveolae (a and c) and lysosomes (b and d) after 24h incubation in bEnd3 cells. Green: NP; red: caveolin1 and lysotracker. Magnification bar: 20 µm.

However, the percentage of colocalization was about 4.68% for blank NP and 0.62% for gH-625-NP. On the other hand, concerning caveolin1, a molecular marker for caveolar structures, no colocalization of gH-625-NP was

observed, while blank NP showed 0.74% of colocalization. These data indicate that the peptide could change the mechanism of nanoparticle uptake by inducing an alternative penetration pathway. To further investigate this issue, we treated cells with cytochalasin D that inhibits macropynocytosis by disrupting microfilaments. Results demonstrate that the uptake of blank NP was drastically reduced after cytochalasin D treatment (Figure 6 A - F).

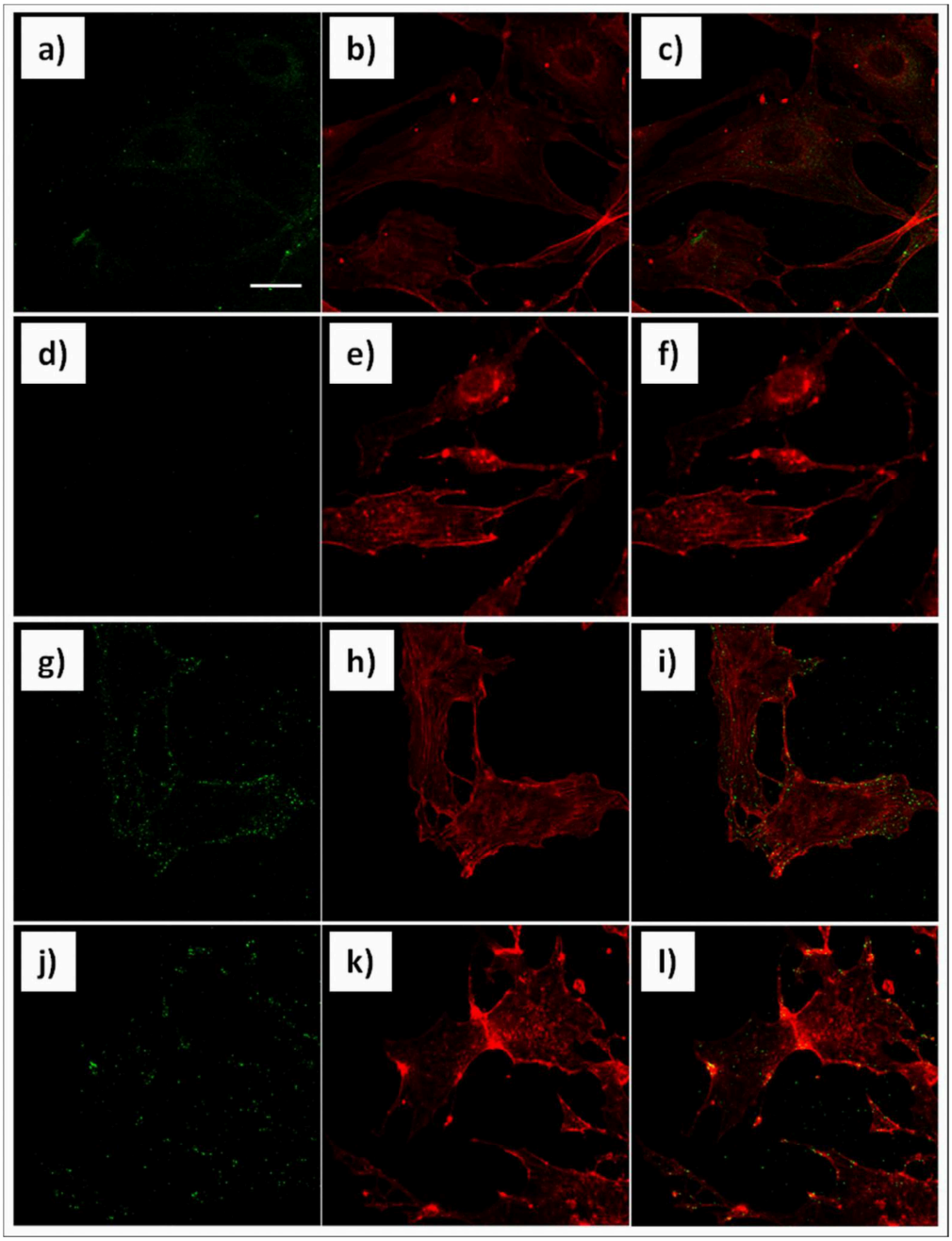

Figure 6. Cytochalasin D treated bEnd3 cells incubated with blank NP (d-f) and gH-625-NP (j-l) for 10 minutes at 37°C. Non-treated control cells incubated with blank NP (a-c) and gH-625-NP (g-i) for 10 minutes at 37°C. Nanoparticles (a, d, g and j); phalloidin stained microfilaments (b, e, h and k); merge (c, f, i and l). Magnification bar: 20 µm.

On the other hand, gH-625-NP uptake was not affected by microfilament depolymerization (Figure 5 G - L). Taken all together these data indicate that blank NP might enter the cells mainly by macropinocytosis. Conversely, gH-625-NP could use a different mechanism to cross cell membrane.

Previous works demonstrated that gH-625 peptide shows a particular tropism for lipidic membranes, which is strongly dependent on its amphipathic nature[13a;13d;13e]. Thus, we hypothesized that the presence of the peptide on the NP surface could enhance its interaction with the cell membrane and promote NP passage through cell membranes. To verify this hypothesis, scanning electron microscopy (SEM) analyses were performed. SEM micrographs showed that, after 5 minutes of incubation, a high number of gH-625-NP was visible on the cell surface (Figure 7 A and B). Furthermore, only some of them were laying on the cell membrane; actually, most of them seemed to be just below the plasma membrane (Figure 6 B). Conversely, very few blank NP were present on the cell surface and some of these formed small aggregates (Figure 7 C and D). Blank NP seemed not to be internalized but simply to lay on the outer cell membrane (Figure 7 D).

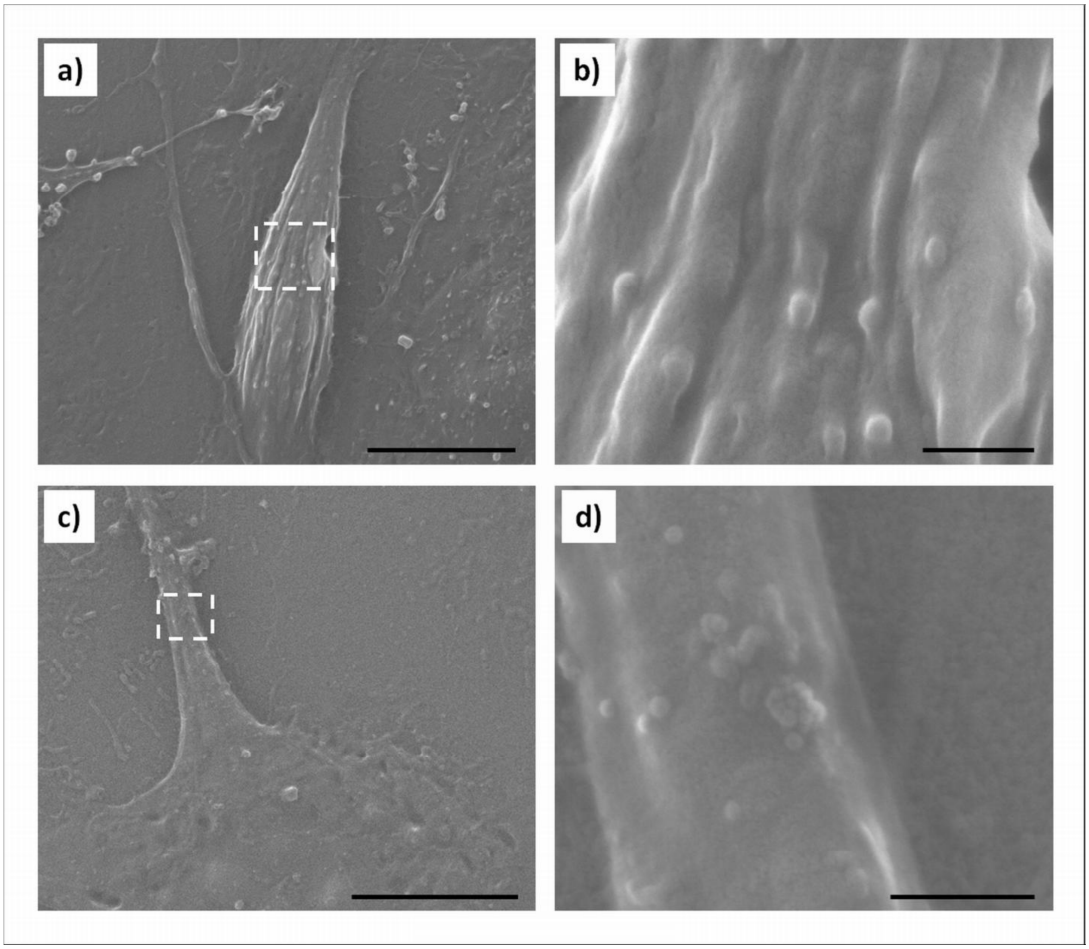

Figure 7. SEM micrographs of bEnd3 cells incubated with gH-625-NP (a and b) and blank NP (c and d) for 5 minutes at 37°C. Dashed squares in figures a and c indicate the zoomed areas shown in figures b and d. Magnification bar: 10 μm (a and c) and 1 μm (b and d).

SEM results suggest a different interaction of gH-625-NP with cell membrane compared to blank-NP. Moreover, accordingly to cell uptake kinetics (Figure 3), these observations indicate a better and more rapid adsorption of gH-625-NP on cell membrane, compared to blank-NP after 10 minutes incubation, probably due to the membrane tropism of the peptide, and, thus, an enhancement of gH-625-NP internalization.

In order to understand if the different behavior of gH-625-NP implied a different intracellular fate of NP, we performed transmission electron microscopy (TEM) analyses. Figure 8 shows TEM micrographs of gH-625-NP and blank NP after 24h incubation with bEnd3 cells. Inside the cells, gH-

625-NP were organized in very small aggregates of 3-4 particles within the cytoplasm, mainly localized in vesicular structures, probably early endosomes (Figure 8A) and multi-vesicular bodies (MVBs) (Figure 8C). On the other hand, for blank-NP, many and larger aggregates associated to vesicular structures within the cytoplasm were observed (Figure 8 B-D). Furthermore, no gH-625- or blank-NP were localized in the nucleus. For obtaining deeper details on the intracellular distribution of gH-625-NP, we followed the formation and the growth of gH-625- or blank-NP aggregates with time by a confocal microscope image analysis. Figure 8 shows gH-625- and blank-NP aggregates within bEnd3 cell cytoplasm after 10 min and 24 h incubation. At early times, gH-625-NP formed a huge number of small aggregates (Figure 9 A and E). Moreover, by increasing the incubation time, the average size of the aggregates remained almost unchanged (Figure 9 B and E). Conversely, for blank NP, at early times, the average size of aggregates increased with time indicating that these NP tend to accumulate in the cell (Figure 9 C, D and F).

Taken altogether, these observations demonstrate a different behavior between gH-625- and blank-NP. In particular, NP conjugation with gH-625 peptide changes NP destination by reducing their accumulation and promoting NP escape/exit from the cell. However, further investigations needed to better understand in which intracellular compartments gH-625-NP are localized and what are the intracellular pathways followed by these functionalized NP that dictate their fate.

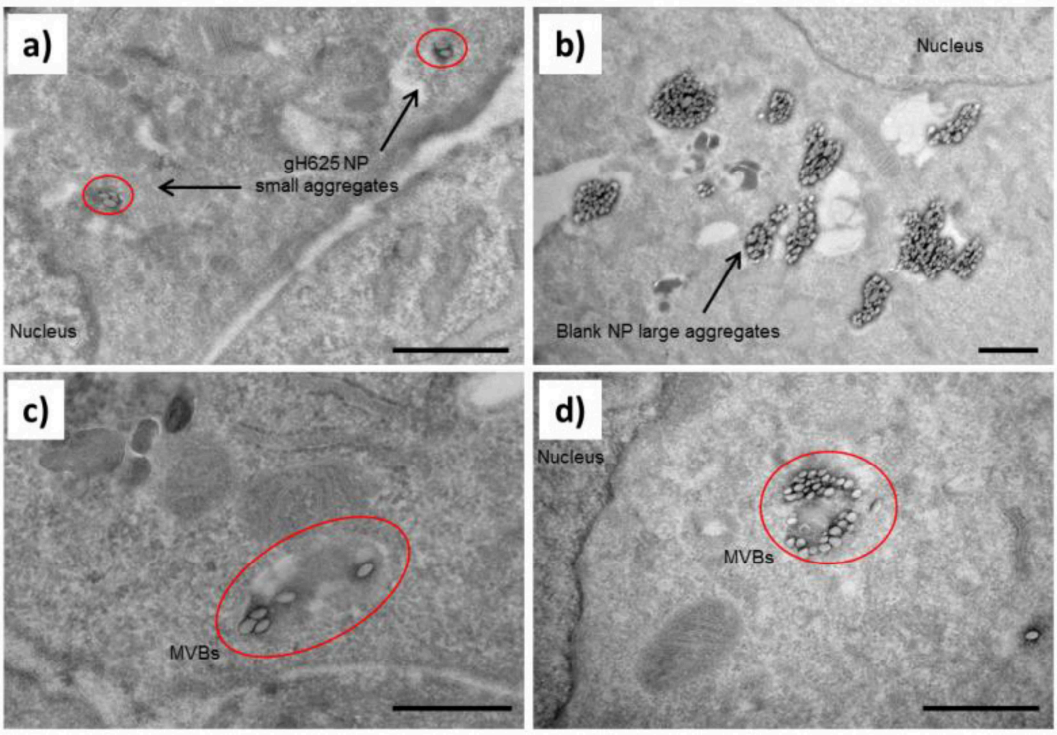

Figure 8. TEM micrographs of bEnd3 cells incubated 24h with gH-625-NP (a and c) and blank NP (b and d) at 37°C. Magnification bar: 1 µm.

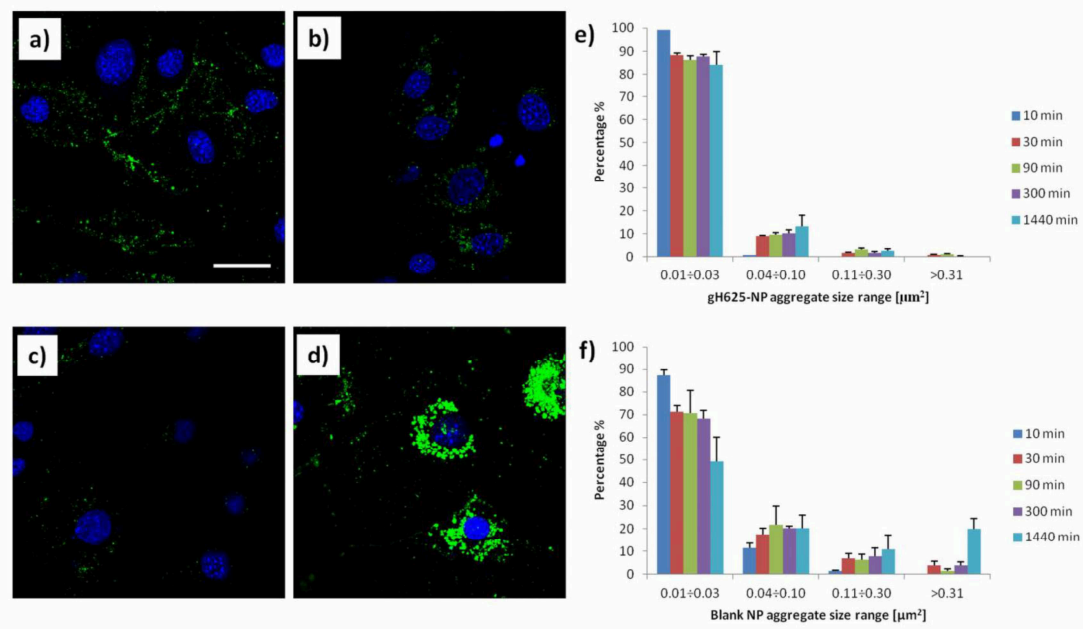

Figure 9. Confocal microscope images of bEnd3 cells incubated with gH-625-NP for 10 min (a) and 1440 min (b) and blank-NP for 10 min (c) and 1440 min (d). Blue: nuclei; Green: NP; Magnification bar: 20 µm. gH-625- (e) and blank-NP (f) aggregates analysis. Charts show the size distribution of NP aggregates at different observation time (10, 30, 90, 300 and 1440 min). NP aggregate sizes were split in four intervals: 0.01÷ 0.03 µm2; 0.04÷ 0.10 µm2; 0.11÷ 0.30 µm2; >0.31 µm2.

3.3.4. Intracellular fate of gH-625-NP

Co-localization with lysosomes over time

To further investigate the effects on intracellular localization of gH-625 conjugated NP, a kinetic of co-localization of NP with lysosomal markers were performed (Figure 10). The results show that both Blank and gH-625 NP co-localize with lysosomes. However, the percentage of co-localization of Blank-NP increases over time, reaching almost 80% after 24 hours of incubation (Figure 10 a), while for gH-625-NP, the percentage of co-localization is lower than Blank-NP and increases up to 6 h. A slight decrease after 24 h is observed. These results demonstrate the low tendency of gH-625 NP to accumulate within the lysosomes.

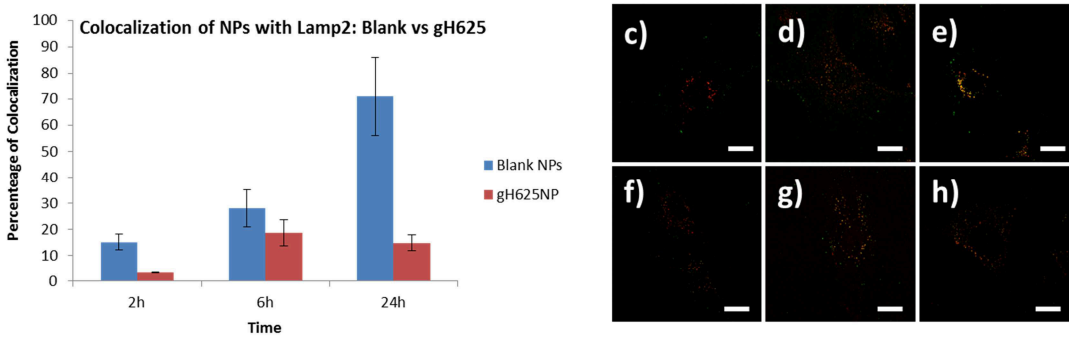

Figure 10. Chart a) shows percentage of co-localization of Blank versus gH-625-NP at different observation time. Confocal microscope images of bEnd3 cell line incubate with Blank-NP (b-d), and with gH-625 (e-g) for 2, 6 and 24 hours. Magnification bar 20 µm

Lysosome swelling

The accumulation of blank NP within the lysosomes affects lysosome size, too. Indeed, an increment in lysosome size up to 1.5 μm^2 is observed after 24h incubation with Blank-NP (Figure 11 a)Conversely, in presence of gH-625-NP, where a scarce co-localization is observed, lysosome size remains almost constant over time (Figure 11 b). These results are in agreement with the analyses of NP aggregate size over time (Figure 9), indicating that the presence of gH-625 peptide on NP surface elude the final lysosomal storage of NPby avoiding the formation of large intracellular aggregates and reducing the enlargement of lysosomes. These data support the thesis based on the

ability of gH-625 peptide to escape the endo-lysosomal compartment (Figure 11).

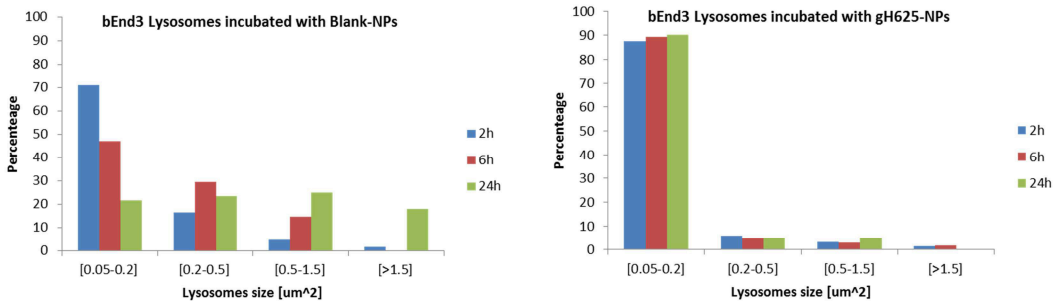

Figure 11. Charts show size distribution of lysosome of cells incubated with Blank-NP (a) and gH-625 (b) at different observation time (2, 6 and 24 hours). Lysosome sizes were split in four intervals: 0.05÷ 0.2:μ^2; 0.5÷ 1.5 : μ^2; >1.5 μ^2.

.

Intracellular trafficking over time

The motion of NP consists of active, ATP-dependent, transport along microtubules and periods of sub-diffusion or diffusion motion in cytosolic compartment. According to the shape drown by NP in cell, trajectories can be classified in two different types: diffusive and pearls-on-a-string. Starting from this concept, we classified as diffusive trajectories (random walk), NP that are able to move freely in cytosol. On the other hand, NP enclosed in vesicular compartment moving along microtubules are described by pearls-on-a-string trajectories. Furthermore, performing MPT experiments up to 24 hours, we discovered a new typology of trajectory that describes a random walk confined displacement. We called this trajectory "random caged". Assuming that "random caged" trajectory represents NP enclosed in lysosomes, the hypothesis is that this behaviour is typical of NP that reach the final lysosomal destination. In fact, once in lysosomes, NP are able to show a random walk-like movement but without leaving the storage compartment. For these reason the displacement is classified as "caged". Time data analysis reveals that only a low percentage of Blank-NP show a diffusive behaviour (random walk), that remains unchanged during the time

of the experiments, suggesting that the most part of NP are not able to move freely in cytosolic compartment (Figure 12 left chart). Conversely, in the presence of peptide, the most part of trajectories are classified as diffusive (Figure 12 right chart). Most importantly, for Blank-NP, we observed a decrease of the percentage of "pearls-on-a-string" and an increase of "random caged" trajectories after 6 and 24 hours of incubation. On the contrary, for gH-625 functionalized NP, the percentage of trajectories has no significant differences during the time of incubation. To explain this result, we assume that after 6 and 24 hours from cellular internalization, Blank-NP reach their final destination in lysosomes, so that their trajectories represent their confinement in these subcellular compartments according to "random caged" behavior. On the contrary, gH-625 conjugated NP behaviour is quite different. The percentage of "random caged" NP remains almost constant during the time of the experimental procedure, suggesting that this percentage (about 20%) is due to the amount of pearls-on-a-string NP that reach final lysosome compartment (Figure 12).

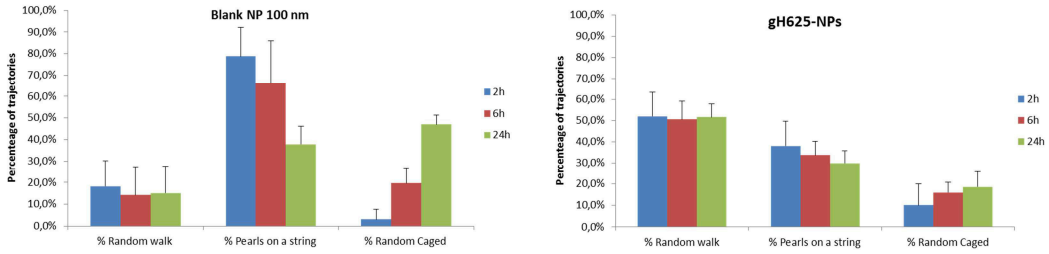

Figure 12. Multiple Particle tracking time resolved experiments.

Intracellular trafficking of gH-625 NP upon gene gun-mediated delivery.

In order to further confirm that the presence of gH-625 peptide allowing endo-lysosomal escape affect the intracellular behaviour of NP, we forced cell membrane crossing by shooting NP with gene gun method.

to allow NP to bypass classical endocytic pathway. As reported in chapter II, we demonstrate that Blank NP, once internalized by cells, show a pearls-on-a-string behaviour prevalently, with a little percentage of random walk

trajectories. On the contrary, if forced to enter the cell by using gene gun method, shot blank NP showed almost exclusively random walk trajectories, suggesting no NP confinement inside endo-lysosomal compartment. In the case of gH-625 NP no significant changes in intracellular trajectories were observed upon delivery of NP by using gene gun method.These data strongly suggest that gH-625 peptide allows NP to escape endo-lysosomal pathway.

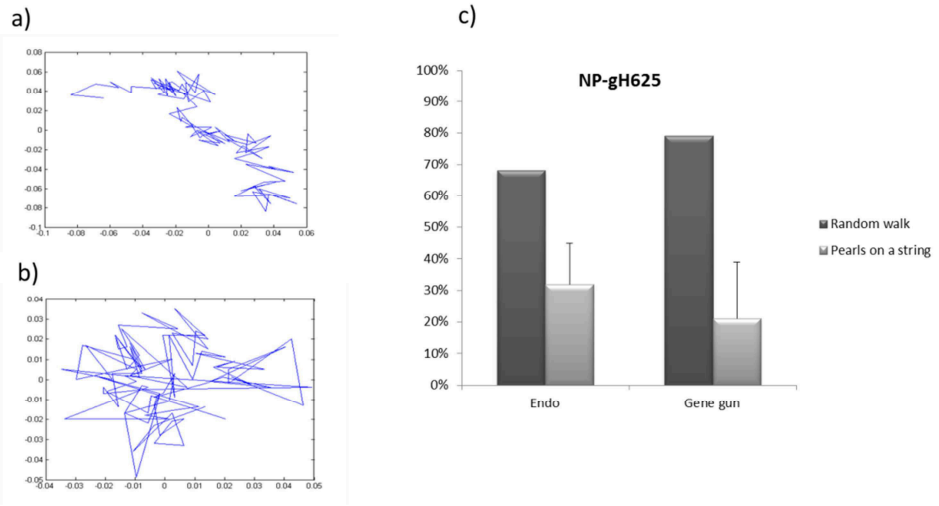

Figure 13. MPT analysis of Endo vs Shot gH-625-NP. Examples of "random walk" (a) and "pearls on a string" (b) trajectories. c) Chart show the percentages of trajectories following "random walk" or "pearl-on-a-string" behaviours.

3.3.8. Effect of gH-625 peptide on 50 nm amine-modified polystyrene NP uptake and cytotoxicity.

The different cellular distribution of Blank and gH-625 conjugated nanoparticles could lead to different impact on cell viability. In order to demonstrate this hypothesis, we tested the effect of gH-625 on cytotoxicity of polystyrene nanoparticles. We chose to use 50 nm PS positively charged NP, known for their higher cytotoxic potential than 100 nm NP on bEnd3 cells. Moreover, recent works reported the cytotoxic effects of 50 nm amine-modified polystyrene NP as a consequence of their localization in lysosomes and interaction with lysosomal components.

Data indicate a reduction of viability of cells treated with 50 ug/ml NP, as expected (Figure 14). On the other hand, after NP shooting, no cytotoxic

effect was observed (Figure 14). Interestingly, after incubation with 50 ug/ml gH-625-NP, only a slight reduction in cell viability was observed, indicating a decrease in NP cytotoxicity (Figure 14). These observations are in general agreement with co-localization results

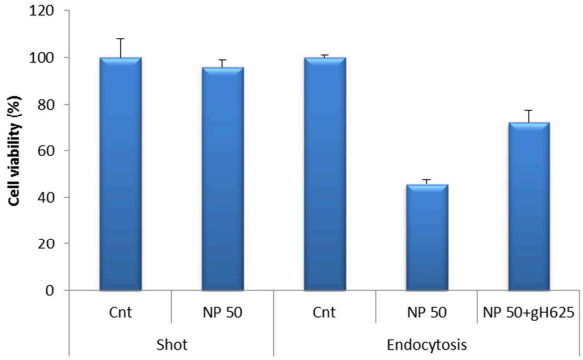

Figure 14 Comparison of cytotoxicityeffect of 50 nm NH_2-NP as a function of different routes of entry.

3.4. Conclusions

The goal of this work was to elucidate the mechanisms that allow gH-625 decorated nanoparticles to escape endo-lysosomal compartment and its impact on cell physiology. The effect on intracellular distribution of gH-625 peptide was verified by performing co-localization with lysosomal markers, this experiment was supported by multiple particle tracking time data analysis. Furthermore, in order to elucidate the mechanism we compare gH-625NP to shot NP, reporting no difference change in NP trajectories.

Most importantly, the conjugation of gH-625 peptide on the surface of 50 nm positively charged polystyrene NP, known to be cytotoxic, allow NP to be safe for cell viability.

Take altogether, these data suggest that the viral fusion virus-derived peptide gH-625 is able to escape endo-lysosomal fate and, hence, could represent a promising strategy for avoiding cytotoxic effects of nanoparticles.

Otherwise, we need further investigations to better elucidate the molecular mechanism used by decorated NP to cross the cell membrane and to identify the possible interactions established between gH-625 NP and cytosolic proteins.

3.5. Materials and methods

Protected Fmoc-amino acid derivatives, coupling reagents and Wang resin were purchased from Fluka, and the other chemicals were purchased from Sigma-Aldrich, Fluka (Buchs, Switzerland) or LabScan (Stillorgan, Dublin, Ireland) and were used as received, unless otherwise stated. Orange fluorescent amine-modified polystyrene, 100 nm, nanoparticles (100 PS NP) and blue fluorescent amine-modified polystyrene, 50 nm, nanoparticles (50 PS NP) were purchased by Sigma-Aldrich.

3.5.1 Peptide synthesis

The peptide gH-625-644 (Ac-HGLASTLTRWAHYNALIRAFGGG-COOH) was synthesized using the standard solid-phase-9-fluorenylmethoxycarbonyl (Fmoc) method as previously reported. [13f] The peptide was obtained with good yields (30-40%).

3.5.2 Peptides conjugation to nanoparticles

A solution of the peptide, EDC (1-Ethyl-3(3-dimethylamino-propyl)-carbodiimide, hydrochloride) and NHS (N-Hydroxysuccinimide) in molar ratio of 4:4:1 was prepared in PBS buffer at pH 7.4, at room temperature under stirring for 30 minutes. NP were conjugated with the preactivated-peptide, in MES 0.1 M buffer at pH 5.5 for 3 hours at room temperature in

presence of Tween 20 and the yield of the reaction was higher than 90%. The peptide-NP were purified from the un-conjugated-NP by exclusion chromatography on a 1 × 18 cm Sephadex G-50 (Amersham Biosciences) column pre-equilibrated in PBS buffer at pH7.4. The fluorescence spectra of peptide-NP and un-conjugated NP were measured in a Cary Eclipse Varian fluorescence spectrophotometer in the same condition. Peptide-NP were prepared with several degrees of functionalization: 25%, 35% and 50%.

3.5.3 Circular Dichroism

CD spectra were recorded using a Jasco J-715 spectropolarimeter in a 1.0 or 0.1 cm quartz cell at room temperature. The spectra are an average of 3 consecutive scans from 260 to 195 nm, recorded with a band width of 3 nm, a time constant of 16 s, and a scan rate of 10 nm/min. Spectra were recorded and corrected for the blank sample.

3.5.4 Size and Z-potential

Measurements of zeta potential and size of gH-625 NP and blank-NP were made with a Zetasizer Nano-ZS (Malvern Instruments, Worcestershire, UK). The measurements were conducted at 25°C using a 3.6 × 1010 NP/ml suspension at pH 4, 7, 8 and 9. All measurements were performed in triplicate for each sample.

3.5.5. Cell culture

Immortalized mouse cerebral endothelial cells, bEnd3 cells (American Type Culture Collection, Manassas, VA) were grown in DMEM with 4.5 g/L glucose, 10% Fetal Bovine Serum (FBS), 3.7 g/L sodium bicarbonate, and 4

mM glutamine, 100 U/ml penicillin and 0.1 mg/ml streptomycin in 100 mm diameter cell culture dish, in a humidified atmosphere at 37°C and 5% CO2. Cells used in all experiments were at passage 28–35.

3.5.6. Co-localization with lysosomes and caveolae

For indirect immunofluorescence, after NP incubation, cells were firstly rinsed twice with PBS to remove non internalised NP and fixed with paraformaldehyde 4% for 20 min. Then, cells were incubated with Triton X100 0.1% in PBS for 10 min and with PBS-BSA 0.5% for 15 min at room temperature (RT). Caveolae were localized by incubating samples first with rabbit anti-caveolin 1 (Abcam) primary antibodies. After primary antibodies incubation, Alexa-fluor 568 goat anti-rabbit secondary antibodies (Molecular Probes, Invitrogen) were used. Afterward, samples were rinsed three times with PBS. For lysosomes localization, LysoTracker Red DND-99 (Molecular Probes, Invitrogen) was used following manufacturer's procedure on non-fixed cells.

Immunofluorescence analyses were performed by means of confocal laser scanning microscope (CLSM)(LSM510, Zeiss), equipped with an argon laser, at a wavelength of 488 nm, and a He–Ne laser, at a wavelength of 543 nm, and 63x objective. Images were acquired with a resolution of 1024×1024 pixels. Colocalization was estimated by an ImageJ software plugin.

3.5.7. Cytochalasin D treatment

To disassemble actin microfilaments, cells were treated with 30 μM cytochalasin D in cell culture medium for 30 min at 37 °C before NP incubation. After cytochalasin D treatment, cells were incubated with a NP suspension for 15 minutes. Then, cells were rinsed with PBS to remove non-

internalized NP, fixed with paraformaldehyde 4% for 20 min and observed by CLSM.

Scanning electron microscopy (SEM): After 10 min incubation with blank NP and gH-625-NP, cells were rinsed with PBS, fixed with 2.5% glutaraldehyde for 2h at 4°C and dehydrated in increasing ethanol series (70%, 80%, 95% and 100%) and by critical point. The samples were gold-sputtered and analyzed by ESEM Quanta 200 (FEI Company) at 25kV and 6.8 mm working distance.

3.5.8. Transmission electron microscopy (TEM)

TEM was performed to precisely localise the intracellular nanoparticles. After 24h incubation with blank NP and gH-625-NP, cells were rinsed with PBS and fixed with 2% paraformaldehyde+0.2% glutaraldehyde for 2h at room temperature. Afterwards, cells were scraped, harvested in centrifuge tubes, embedded in 12% gelatine solution in PBS and infused in 2.3 M sucrose at 4°C. Sections were cut with a Leica Cryo-ultramicrotome and examined with Leica EM FC7.

3.5.9 Quantification of NP aggregates

To measure the size of NP aggregates within cell cytoplasm, bEnd3 cells were incubated with NP suspension for 30, 90, 1440 minutes at 37°C. After incubation, cells were rinsed twice with PBS, fixed with paraformaldehyde 4% for 20 min and observed by confocal microscope (Leica). Images were analyzed by an ImageJ software plugin. About 50 cells per each sample were analyzed. The size distribution of NP aggregates was split in four intervals (0.01÷ 0.03 μm2; 0.04÷ 0.10 μm2; 0.11÷ 0.30 μm2; >0.31 μm2) and data reported as percentage of NP aggregates respect to the total number of NP aggregates per cell.

Statistical analyses: Quantitative data were reported as mean ± standard deviation (SD). Statistical analyses were performed using a one-way analysis of variance (ANOVA). Results repeats were compared by analysis of variance (ANOVA), and a p value < 0.05 was considered statistically significant.

3.5.10. Multiple particle tracking

Images of shot and endo 100 nm PS NP in End3 cells were collected in time-lapse for about 100 s with a sampling time of 1 second by using a widefield fluorescence microscope (Olympus Cell-R, 60x oil immersion objective, NA = 1.35). Tracking algorithm has been described in details elsewhere [Guarnieri et al., Journal of Nanoparticle Research 2011]. NP trajectories were built and then the mean square displacement (MSD) was calculated and correlated with the NP diffusion by the equation (1) ,

$$MSD = 4Dt^{\alpha}$$

where D is the diffusion coefficient and α represents the time dependence. By fitting the MSD curve of each tracked bead by using equation (1), informations concerning the nature of particle motion into the cells were gained. Nanoparticles, exhibiting MSD curve that undergoes a power law with exponent minor or equal to unity, were classified as Brownian ($\alpha=1$) or sub-diffusive ($\alpha<1$). Particles presenting MSD, whose dependence on time was well described by the power law with $\alpha>1$, were indicated as super-diffusive. In particular, about the α coefficient we can distinguish three critical cases: $\alpha = 0$, for immobile NP (displacement does not change with time); $\alpha = 1$, for a randomly moving NP; $\alpha = 2$ for a NP moving in a straight line at a constant velocity. For $1< \alpha < 2$ an overlap between random and straight motion is found, reflecting the NP active motion along the filaments due to the action of molecular motors. The percentages of randomly

moving NP ($\alpha \leq 1$) and transported NP ($1 < \alpha < 2$) were evaluated and compared for shooting and endocytosis.

3.5.11. Quantification of internalized nanoparticles

To evaluate the number of endo and shot NP within cells, after NP incubation, cells were roughly rinsed with PBS, trypsinized and counted by Neubauer chamber. Afterward, cells were centrifuged and the pellets were lysed with lysis buffer. Cell lysates were analyzed by a spectrofluorometer (Perkin–Elmer, USA) to measure the amount of internalized PS-NP. Data were reported as NP number normalized to the number of cells. Samples that had the same number of NP per cell were used and compared each other for cytotoxicity Fig.S1

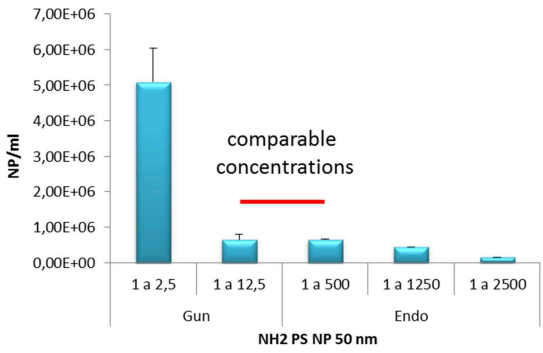

Figure S1. Quantification of Blank NP: shot vs endo

3.5.12. *In vitro* cytotoxicity

bEnd3 cell viability was quantified by Alamar Blue Assay and compared to non-treated cells, which were used as a control. Briefly, 3×10^4 cells were seeded on a 35 mm cell culture dish and incubated 24 h with NP suspensions to allow endocytosis. Conversely, for NP shooting, cells were shot with NP by gene gun, washed roughly with PBS and, then, allowed to recover for 24 h

at 37°C. After recovery, cells were trypsinized, counted and seeded on fresh 35 mm cell culture dishes. Alamar Blue Assay was performed according to the manufacturer's procedure at 1 day after NP exposure. Absorbance of Alamar Blue reagent solution was read at 570 nm and 600 nm by a plate reader (Perkinelmer). Data were reported as percentage of viable cells normalized to non-treated cells.

References

1. Liao, Z., Cimakasky, L. M., Hampton, R., Nguyen, D. H., & Hildreth, J. E. (2001). Lipid rafts and HIV pathogenesis: host membrane cholesterol is required for infection by HIV type 1. *AIDS research and human retroviruses*, *17*(11), 1009-1019.
2. Nel, A. E., Mädler, L., Velegol, D., Xia, T., Hoek, E. M., Somasundaran, P., Thompson, M. Understanding biophysicochemical interactions at the nano–bio interface. *Nature materials*, *8*(7), 543-557. (2009).
3. Różycki, B., Boura, E., Hurley, J. H., & Hummer, G. (2012). Membrane-elasticity model of Coatless vesicle budding induced by ESCRT complexes. *PLoS computational biology*, *8*(10), e1002736
4. Daniela Guarnieri, Annarita Falanga, Ornella Muscetti, Rossella Tarallo, Sabato Fusco, Massimiliano Galdiero, Stefania Galdiero*, Paolo A. Netti*, 2012. *Shuttle-mediated nanoparticle delivery to the blood brain barrier*. DOI: 10.1002/smll.
5. Zhao, F., Zhao, Y., Liu, Y., Chang, X., Chen, C., & Zhao, Y. (2011). Cellular uptake, intracellular trafficking, and cytotoxicity of nanomaterials. *Small*, *7*(10), 1322-1337.
6. Fröhlich, E., Meindl, C., Roblegg, E., Ebner, B., Absenger, M., & Pieber, T. R. (2012). Action of polystyrene nanoparticles of different sizes on lysosomal function and integrity. *Particle and fibre toxicology*, *9*(1), 1-13.
7. Huynh, C., Roth, D., Ward, D. M., Kaplan, J., & Andrews, N. W. (2004). Defective lysosomal exocytosis and plasma membrane repair in Chediak–Higashi/beige cells. *Proceedings of the National Academy of Sciences of the United States of America*, *101*(48), 16795-16800.
8. Wang, F*., et al.* The biomolecular corona is retained during nanoparticle uptake and protects the cells from the damage induced by cationic nanoparticles until degraded in the lysosomes. *Nanomedicine-Nanotechnology Biology and Medicine* 9, 1159-1168 (2013).
9. Vecchio, G., Galeone, A., Brunetti, V., Maiorano, G., Rizzello, L., Sabella, S., ... & Pompa, P. P. (2012). Mutagenic effects of gold nanoparticles induce aberrant phenotypes in< i> Drosophila melanogaster</i>. *Nanomedicine: Nanotechnology, Biology and Medicine*, *8*(1), 1-7.
10. Kim, J.A*., et al.* Correction to Low Dose of Amino-Modified Nanoparticles Induces Cell Cycle Arrest. *Acs Nano* (2013).
11. Guarnieri, D*., et al.* Shuttle-Mediated Nanoparticle Delivery to the Blood-Brain Barrier. *Small* 9, 853-862 (2013).

12. G. Vitiello, A. Falanga, M. Galdiero, D. Marsh, S. Galdiero and G. D'Errico. *Biochim. Biophys.* Acta 1808, 2517.(2010)
13. B. DiBlasio, S. Galdiero, M. Saviano, G. DeSimone, E. Benedetti, C. Pedone, W. A. Gibbons, R. Deschenaux, E. Rizzarelli and G. Vecchio, *Supramolecular Chemistry* 1996 *7*, 47

4. CHAPTER III

BIO-INSPIRED ENGINEERED NANOPARTICLES TO ENHANCE DELIVERY TO THE BLOOD BRAIN BARRIER

3.1. ABSTRACT

Due to the presence of specialized endothelial cells, the blood brain barrier (BBB) is a selective physiological barrier able to protect the brain from pathogens and unwanted substances. On the other hand, this selectivity represents the main obstacle for delivery drugs to the central nervous system (CNS). To overcome this limitation, the use of nanoparticles (NP) could be a promising strategy to deliver therapeutic agents across the BBB thus improving the efficacy of therapies for several CNS diseases.
A method to further enhance NP delivery through the BBB is to modify their surface with bioactive peptides such as cell-penetrating peptide (CPPs). CPPs are a group of short peptides shared by common features as amphipathic nature, net positive charge, theoretical hydrophobicity and helical moment that allow them to interact with lipidic membranes. The ability of CPPs to penetrate cell membranes and transport a large variety of cargo molecules/material inside cells is widely reported, although there are controversies regarding the uptake mechanisms used by CPPs-functionalized carriers.
In this work, first we optimized an *in vitro* model of BBB in order to investigate the effect of NP characteristics on the interaction with the BBB to rank them in order of efficiency, then, we studied the effect of NP surface decoration with a novel CPP sequence (gH-625), derived from the glycoprotein H of the Herpes Simplex virus type 1 envelope, on promoting NP uptake and crossing of the BBB.
In particular, polystyrene nanoparticles with variable size and surface charge have been tested with bEnd.3 cell monolayer, grown on a Transwell system, in order to identify the parameters regulating the nanoparticles/BBB interaction and, thus, the nanoparticle capability to pass through the endothelial barrier. Cells were next exposed to fluorescent aminated polystyrene NP functionalized with gH-625 peptide sequence. Transcytosis and uptake kinetic of gH-625-NP were investigated. The results showed that

the presence of gH-625 peptide enhances BBB crossing compare to non-functionalized NP. These data suggest that the decoration of nanoparticle surface with gH-625 peptide sequence enhances BBB overcoming. In this direction, this study could provide a useful strategy to design nanocarriers for the delivery of therapeutic agents to the CNS.

3.2. Introduction

Neurological disorders contribute significantly to the global burden of disease and are likely to increase in the coming years due to an aging population; thus, significant efforts have been devoted towards the development of improved therapies for central nervous system (CNS) diseases. However, despite these efforts, treatments remain limited due to the inability of therapeutic agents to effectively cross the blood-brain-barrier (BBB).[1] The BBB is a dynamic barrier protecting the brain against invading organisms and unwanted substances; thus, the BBB is a formidable obstacle to the effective delivery of drugs to the CNS and poses a major challenge to drug development efforts (Figure 1).[2] Therefore, the development of effective strategies to enhance drug delivery to the brain, that is, the availability of a drug at its site of action in the brain for sufficient time to exert its biological effect, is the ultimate aim of any CNS clinical and pharmaceutical program.

Most strategies to transport pharmaceutical compounds inside the CNS causes disruption of the anatomical texture of the BBB therefore impairing its natural function. Effective delivery approaches should be cautiously assessed considering their impact on the overall protective function of the BBB. It is now well-known that there are several invasive or non-invasive transport routes by which brain drugs cross the BBB.[2] The invasive approaches consist of a temporary disruption of the BBB allowing the entry of a drug into the CNS or the direct drug delivery by means of intraventricular or intracerebral administration[3] while the non-invasive ones involve the systemic application

of colloidal drug carriers undergoing a receptor or adsorptive mediated transcytosis mechanism[4] or the passing of the BBB via intranasal delivery.[5]

Nanocarriers (linear and hyperbranched polymers, dendrimers, liposomes, micelles, niosomes and cyclodextrins)[6] are an emerging class of drug delivery systems that can be easily tailored to deliver drugs to various compartments of the body, including the brain.

Nanocarriers possess unique features due to their size and the possibility of being functionalized with multiple copies of the drug molecule of interest. In particular, they allow the transport of a range of drugs, therefore modification of nanocarrier surface properties ensues. These properties make nanocarriers an attractive alternative to existing methods for transporting drugs across the BBB. Despite a large variety of nanocarriers developed so far for cellular internalization, it is noteworthy that only amphiphilic molecule-formed liposomes and polymeric nanoparticles have been extensively exploited for brain drug delivery.[7] Several of those systems are now in clinical trials mainly for anticancer drug delivery.

An essential role for nanoparticles is to help drugs gaining increased water stability, better pharmacokinetics, reduced toxicity and improved therapeutic efficacy.[8]Because of nanoparticles versatility, diagnostic and therapeutic drugs can be either physically encapsulated or covalently conjugated to nanoparticles. In this context, the conjugation of therapeutic molecules to shuttles that can cross the BBB and thus carry drugs into the brain emerges as an attractive alternative. A key mechanism to further enhance nanoparticle delivery is to improve their transport by modification of their surface with bioactive peptides such as cell-penetrating peptides (CPPs). CPPs are a group of relatively short peptides (5-40 amino acids) deriving either from natural sources or from synthetically designed constructs, that are able to penetrate cell membranes and transport a large variety of cargo molecules/materials inside cells.[9] While individual CPPs differ in length and sequence, they all share some common features, which include their amphipathic nature, net

positive charge, theoretical hydrophobicity and helical moment, the ability to interact with lipidic membranes, and to adopt a distinct secondary structure upon association with lipids.[10]The general application of CPPs in cellular delivery has been hampered by the controversy regarding the uptake mechanism used by these peptides. The major dogma has been that CPPs enter cells by a receptor and energy-independent process although the exact mechanism is not yet fully understood; but it is now evident that for most CPPs, endocytosis is an almost exclusive mechanism of internalization. By following this pathway, cargos transported by CPPs, such as therapeutic molecules or functionalized nanoparticles, may experience lysosomal pH (around 5), which can strongly accelerate drug degradation, and/or nanoparticle accumulation within late endosomes by making less effective the transport of nanoparticles through the BBB.

Although several studies demonstrate the effectiveness of CPPs, such as TAT[11], in promoting the transport of nanoparticles across the BBB, the compelling need of enhancing delivery to the brain makes it essential to exploit novel molecules which use different internalization mechanisms. Moreover, the controversy regarding the mechanism of action and the growing number of peptides with cell-penetrating properties has increased the challenge. Recently, great attention has been devoted to the study of hydrophobic peptides that efficiently traverse biological membranes, promoting lipid membrane-reorganizing processes, such as fusion or pore formation and thus involving temporary membrane destabilization and subsequent reorganization.[12]

The nineteen residues peptide gH-625, was previously identified as a membrane-perturbing domain in the glycoprotein gH of *Herpes simplex* virus type I;[13] gH-625 interacts with biological membranes, contributing to the merging of the viral envelope and the cellular membrane; it is able to traverse the membrane bilayer and to transport a cargo into the cytoplasm.[14] We already reported the ability of the peptide gH-625 to transport quantum dots

inside the cytoplasm in an efficient way and only partially involving endocytic pathways.[14a]

Here we report the effect of gH-625 on the penetration of 100 nm polystyrene nanoparticles (NP) through an *in vitro* BBB model based on bEnd3, an immortalized mouse cerebral endothelial cell line.

First we optimized a BBB *in vitro* model in order to study the capability of NP to cross the brain endothelium as a function of feature (e.g. size, surface charge, and functionalization)(as deeply described in the Methods paragraph).Then we demonstrated that, by opportunely modifying surface properties, it is possible to change the fate of nanoparticles. In particular, we verified that gH-625 conjugation enhances nanoparticles transport across the BBB, thereby enhancing the CNS bioavailability of an eventual drug. This study holds importance for treatment of brain infections and tracking of nanoparticles *in vivo*, a step closer to the development of a clinically applicable nanocarrier for treatment as well as monitoring brain related disorders.

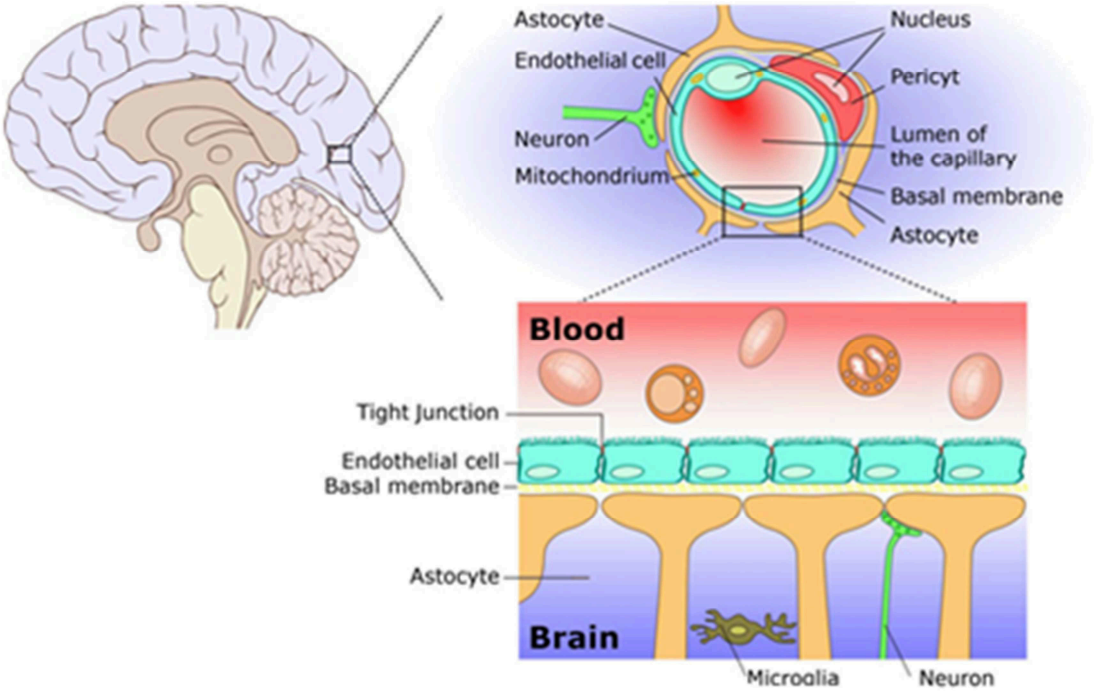

Figure.1 Schematic representation of blood-brain barrier.

3.3. The building blocks of the BBB

3.3.1. Tight junctions

Junction complex in the BBB comprises tight junction (TJ) and adherens junction (AJ).

TJ constitute the most apical intercellular junctional complex in polarized endothelium, with three key biological functiones: a barrier to paracellular diffusion of blood-borne polar substances, a fence preventing the lateral diffusion of lipids and integral proteins, thus maintaining cellular polarization (Figure 2).

TJ consists of three integral membrane proteins, namely, claudin, occludin, and junction adhesion molecules, and a number of cytoplasmic accessorize proteins as ZO-1, ZO-2, ZO-3, cingulin and others. Cytoplasmic proteins are able to link membrane proteins to actin, which is the primary cytoskeleton protein for retain structural and functional integrity of the endothelium. AJ are composed of a cadherin-catenin complex and its associated proteins[17-18].

3.3.2. Claudins

At least 24 members have been identified in claudin family, both in mouse and human.

Claudins are the main component of the TJ, are localized at TJ strands, are 22KDa phosphoprotein and have four transmembrane domanins. Claudins bind homotypically to claudins on adjacent endothelial cell to form primary seal of the TJ Rif (furuse et al 1999). Claudins bind trought the carboxyl terminal, the cytoplasmatic protein ZO-1, ZO-2 and ZO-3. It has has been reported that claudin 1 and 5 toghether with occludin are expressed TJ in brain, loss of claudin 1, but not 5 from cerebral vessels was demonstrated

under pathologic conditions such as tumor, stroke and inflammation as well as in vitro[17-18].

3.3.3. Occludin

Occludin is a 65-KDa phosphoprotein, larger then claudin. Shows no aminoacid sequence similar to the claudins, and as the claudins, occludin has transmembrane domanins.

Occludin is composed by four transmembrane domains, a long COOH-terminal domain and a short NH_2-terminal cytoplasmatic domain. The two extracellular loops of claudin and occluding originating from neighboring cells form the paracellular barrier of TJ. The occludin trought the cytoplasmatic domain is directly associated with ZO proteins.

Occludin expression is major in brain endothelial cells than in non neural tissues, furthermore seems to be a regulary protein that can alter paracellular permeability.

Forming an heteroplymers, occludin and claudin, form intramembranous strands, these strands have been proposed to contain channels that allow to selective diffusion of ions and idrophilic molecules. Togheter, claudins and occludins form the extracellular component of TJs and are both required for the BBB formation[18-19].

3.3.4. Junctional adhesion molecules

Junctional adhesion molecules (JAM) are approximately 40KDa single transmembrane domain proteins.

JAM belong to the immunoglobulin superfamily, they extracellular portion has two immunoglobulin-like loops formed by disulphide bonds.

The expression of JAM in human BBB is yet to be explored. It is involved in cell-to cell adhesion and monocyte transmigration trough BBB[19].
However more have to be investigated to unfold its function in the BBB.

3.3.5. Cytoplasmatic accessory proteins

The accessory proteins of TJ complex belong to the family of well known as membrane-associated guanylate kinase-like proteins (MAGUKs). They are charachterized by the presence of three PDZ domanis (PDZ1, PDZ2 and PDZ3), one SH3 domain, and one guanyl kinaslike (GUK) domain.
All these domains are useful to bind molecules and thus playing a central role in organizating proteins at the plasma membrane.
Is reported that the PDZ1 domain of ZO-1, ZO-2 and ZO-3 bind directly the COOH-terminal of claudins. JAM was also recently shown to bind directly ZO-1 and other PDZ-containings protein, most importantly, actin, wich is the main cytoskeleton protein, is bind to COOH-terminal of ZO-1 and ZO-2 and this complex cross link the transmembrane elements, thus providing support to the endothelial cells[17-18].

3.3.6. Adherens junctions

The formation of AJs is promoted by homophilc interactions between the extracellular domains of calcium-dependent cadherin on the surface of adjacent cells. In order to form adhesive contact between the cells, the membrane protein cadherin, associated with the intermediatery protein catenins, join the cytoskeleton actin. AJs components have been demonstrated in intact microvessels of the BBB in rat.
TJ and AJ components are known to interact with ZO-1 and catenins, and influence TJ assembly[20].

3.3.7. Role of astrocytes

Astrocytes are so called star cells. They perform many functions, including biochemical support of endothelial cells that form the blood–brain barrier, provision of nutrients to the nervous tissue, maintenance of extracellular ion balance, and a role in the repair and scarring process of the brain and spinal cord following traumatic injuries[18].

3.3.8. Pericytes

Pericytes (PCs) are cells of microvessels including capillaries, venules and arterioles that wrap around endothelial cells. It has been widely demonstrated that PCs provide support and vasodynamic capacity to the microvasculature, thus playing a key role in the structural stability of the vessel wall. In vitro studies has been conducted in order to understand the role of PCs in angiogenesis and differentiation of BBB, the results support the thesis that PCs have pivoltal role in integrity and genesis of the BBB[18].

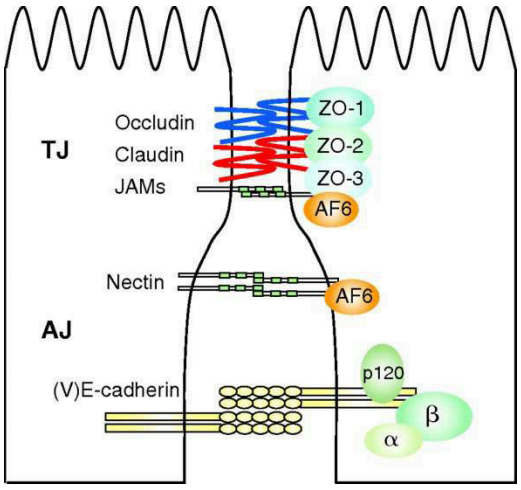

Figure.2 Schematic representation of tight junction complex.

3.4. Results and Discussion

3.4.1. Uptake kinetics and *in vitro* BBB crossing of peptide conjugated nanoparticles.

To study the effect of surface functionalization with gH-625 on NP internalization, we performed NP uptake experiments. Figure 3A shows that after 10 minutes of incubation, both functionalized and blank NP were internalized by bEnd3 cells and the number of internalized nanoparticles increases as a function of incubation time. However, the amount of internalized gH-625-NP is higher than blank NP and this effect is more evident at early time of NP uptake kinetic. While after longer incubation time the amount of internalized NP is quite similar, probably due to the saturation of the uptake mechanism mediated by the gH-625 peptide.

bEnd3 cells are able to form a confluent monolayer that mimics permeability properties of primary culture models of early passages. We tested the ability of gH-625 peptide to enhance NP crossing of a bEnd3 confluent monolayer. Data reported in Figure 3B show that gH-625-NP cross more efficiently the endothelial layer than blank NP. More precisely, the permeability (P) of the monolayer was (0.43 ± 0.02) × 10-6 cm/sec for gH-625-NP, almost two fold higher than P value reported for blank-NP ((0.24 ± 0.02) × 10-6 cm/sec)(Table 2). These data are in agreement with cell uptake kinetic results. In fact, by focusing at early incubation time, also the uptake rate of peptide-conjugated NP was approximately double compared to blank NP (see the insert in Figure 3A). Moreover, no changes in BSA-TRITC permeability were observed after exposure to both blank and gH-625-NP, indicating that these NP did not perturb the integrity of the cell monolayer in the experimental conditions used for the assay (data not shown).

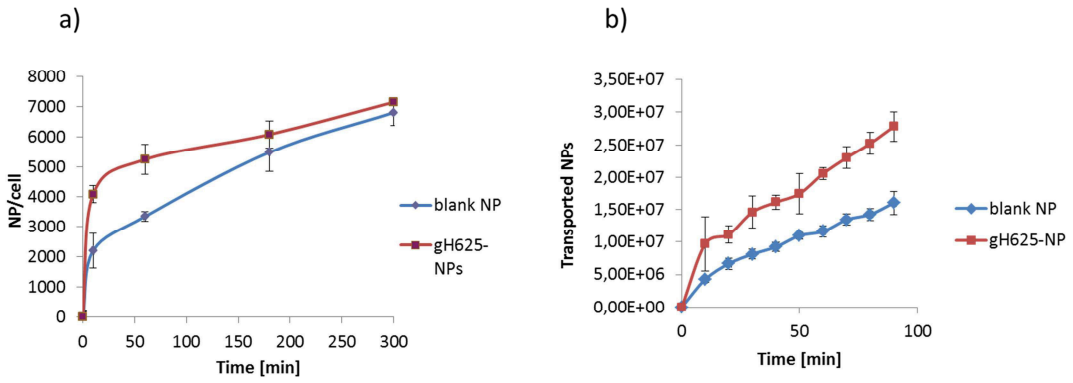

Figure 3. Uptake kinetics of blank and 35% functionalized gH-625-NP in bEnd3 cells (a). Effect of peptide functionalization in NP crossing of a confluent bEnd3 cell monolayer (b).

3.5. Conclusions

The aim of the present work was to verify if synthetic peptides derived from viral membranotropic sequences can be used successfully to deliver biologically active substances inside the BBB in order to pose the basis for developing new effective strategies for drug delivery into the brain. The HSV gH-derived-peptide was covalently bonded with polystyrene nanoparticles and investigated for the ability to translocate through the BBB in an *in vitro* model. The functionalized nanoparticles were thoroughly characterized using a variety of complementary techniques to gain a better understanding of their properties and showed that gH-625-NP only slightly modified the particle sizes with a z-potential indicative of colloidal stability at pH 7. gH-625-NP translocated efficiently across cell membranes and cell internalization does not seem to exclusively involve classical endocytosis mechanisms. In fact, conjugation with the gH-625 facilitated the delivery of nanoparticles across the BBB, leading to significant higher cell uptake and crossing. To the best of our knowledge, the gH-625 represent a cell translocation motif never reported before in a BBB *in vitro* analysis and could be applied to the design of a drug delivery system homing to the brain and bypassing the endocytosis entrapment. Therefore, these novel nanocarriers could be regarded as a

promising strategy to design delivery systems for administration of therapeutical compounds to the brain, deserving further investigations to more precisely characterize the mechanism by which gH-625 crosses the BBB.

3.6. Experimental Section

3.6.1. Materials

Protected Fmoc-amino acid derivatives, coupling reagents and Wang resin were purchased from Fluka, and the other chemicals were purchased from Sigma-Aldrich, Fluka (Buchs, Switzerland) or LabScan (Stillorgan, Dublin, Ireland) and were used as received, unless otherwise stated. Orange fluorescent amine-modified polystyrene, 100 nm, (NP-NH2) were purchased by Sigma-Aldrich.

3.6.2. Peptide synthesis

The peptide gH-625-644 (Ac-HGLASTLTRWAHYNALIRAFGGG-COOH) was synthesized using the standard solid-phase-9-fluorenylmethoxycarbonyl (Fmoc) method as previously reported. The peptide was obtained with good yields (30-40%). *Peptides conjugation to NP:* A solution of the peptide, EDC (1-Ethyl-3(3-dimethylamino-propyl)-carbodiimide, hydrochloride) and NHS (N-Hydroxysuccinimide) in molar ratio of 4:4:1 was prepared in PBS buffer at pH 7.4, at room temperature under stirring for 30 minutes. NP were conjugated with the preactivated-peptide, in MES 0.1 M buffer at pH 5.5 for 3 hours at room temperature in presence of Tween 20 and the yield of the reaction was higher than 90%. The peptide-NP were purified from the un-conjugated-NP by exclusion chromatography on a 1 × 18 cm Sephadex G-50 (Amersham Biosciences) column pre-equilibrated in PBS buffer at pH7.4.

The fluorescence spectra of peptide-NP and un-conjugated NP were measured in a Cary Eclipse Varian fluorescence spectrophotometer in the same condition. Peptide-NP were prepared with several degrees of functionalization: 25%, 35% and 50%.

Quantification of nanoparticle uptake kinetic: To evaluate cell uptake of NP as a function of NP surface functionalization with gH-625 peptide, about 5·104 cells were seeded in a 96-well. Blank-NP and gH-625-NP were dispersed in cell culture medium at the final concentration of 3.6 × 1010 NP/ml. Cells were incubated with NP suspensions for 0, 10, 60, 180 and 300 minutes. After incubation, cells were rinsed with PBS and lysed with 1% Triton X100 in PBS. Cell lysates were analyzed by a spectrofluorometer (Wallac 1420 Victor2™, Perkin–Elmer, USA) to measure the amount of internalized NP.

3.6.3. Polystyrene nanoparticles

Nanoparticles used in this work are the following: green and red fluorescent polystyrene nanoparticles with diameters respectively of 44 (NP44) and 100 (NP100) nm (Duke Scientific Corporation).

Yellow-green fluorescent carboxylate-modified polystyrene nanoparticles, 100 nm, (NP-COOH) (Life Technologies, USA).

Orange fluorescent amine-modified polystyrene nanoparticles, 100 nm, (NP-NH_2) (Sigma-Aldrich).

Morphology of polystyrene nanoparticles is verified by transmission electron microscopy (TEM) (Figure 1).

To elucidate the colloidal stability of nanoparticles, measurements of the zeta potential and of the hydrodynamic radius (D_H) are carried out with a Zetasizer Nano-ZS (Malvern Instruments, Worcestershire, UK) at 25 °C by using a nanoparticle concentration, corresponding to 0.9×10^{10} NP/ml. At least

3-5 measurements of all samples should be performed to have a statistical significance.

3.6.4. Cell culture

Immortalized mouse cerebral endothelial cells, bEnd.3 cells (American Type Culture Collection, Manassas, VA) are grown in Dulbecco's Modified Eagle's Medium (DMEM) with 4.5 g/l glucose, 10% Foetal Bovine Serum (FBS)(Gibco), 4 mM glutamine (Gibco), 100 U/ml penicillin and 0.1 mg/ml streptomycin (Gibco) in a 100 mm diameter cell culture dish (Corning Incorporated, Corning, NY), in a humidified atmosphere at 37 °C and 5% CO_2. Cell culture medium is changed every 3-4 days and cells are split after reaching confluency. Phosphate buffered saline solution (PBS) and trypsin/EDTA solution are from Gibco. Cells used in all experiments are at passage 28–35. To evaluate nanoparticle cellular uptake, 5×10^4 cells are seeded in a 96-well. For permeability experiments cells were seeded on Transwell permeable inserts as described below.

3.6.5. TEER measurements

Tight junction formation and BBB functionality are assessed by transendothelial electrical resistance (TEER) across the filters using an electrical resistance system (ERS) with a current-passing and voltage-measuring electrode (Millicell-ERS, Millipore Corporation, Bedford, MA). TEER ($\Omega \bullet cm^2$) is calculated from the displayed electrical resistance on the readout screen by subtraction of the electrical resistance of a filter without cells and a correction for filter surface area (Table 2).

Permeability experiments

1. Seed 3 × 10^4 cells in 150 µl of complete medium on Transwell permeable inserts (6.5 mm in diameter, 3 µm pores size) (Corning Incorporated, Corning, NY), add 400 µl of complete medium in the basal compartment of the Transwell system and allow them to grow up to 7 days. Change cell culture medium every 3-4 days.
2. Dilute nanoparticles in complete cell culture medium w/o phenol red at the final concentration of 0.002% solids, corresponding to 4.2 × 10^{11} for 44 nm NP and 3.6 × 10^{10} NP/ml for NP100, NP-COOH and NP-NH_2, and sonicate NP suspension for 3 min prior to use.
3. A schematic representation of the system used for permeability experiments is reported in Figure 2.

3.6.6. Fluorescent probes

1. Albumin from Bovine Serum (BSA), Alexa Fluor® 488 Conjugate (Life Technologies, USA) is used as a standard fluorescent probe for permeability measurements.
2. Working solutions of fluorescent probes are prepared by dissolving the BSA in complete medium w/o phenol red at the final concentration of 0.5 mg/ml.
3. Solution is sonicated for 2-3 min to promote BSA dissolution.

3.6.7. Indirect immunofluorescence

1. 4% paraformaldehyde solution is prepared by dissolving paraformaldehyde powder in PBS at about 100 °C under stirring. When the solution becomes transparent, make aliquots of about 4-5 ml in 15 ml conic tubes and store them at -20 °C.

2. 0.1% Triton X100 solution is prepared by diluting Triton X100 (Sigma) in PBS under stirring. Store the solution at room temperature.
3. Prepare PBS-BSA solution by dissolving 0.5% (w/v) bovine serum albumin (BSA) (Sigma) in PBS at room temperature.
4. Tight junctions are localized by incubating samples first with mouse anti-claudin 5 primary antibodies (Invitrogen, Life Technologies) diluted 1: 100 in PBS-BSA 0.5% and then with Alexa-fluor 488 anti-mouse secondary antibodies diluted 1: 500 in PBS-BSA 0.5% (Invitrogen, Life Technologies).
5. Rabbit anti-EEA 1 primary antibodies (ABR) diluted 1: 200 in PBS-BSA 0.5% are used with Alexa-fluor goat anti-rabbit secondary antibodies diluted 1: 500 in PBS-BSA 0.5% (Invitrogen, Life Technologies) to label early endosomes.
6. The excitation wavelengths of secondary antibodies are 488 nm and 568 nm for samples treated with red and green fluorescent nanoparticles, respectively.

3.7. Methods

3.7.1. Quantification of nanoparticle uptake

1. To evaluate cellular uptake of nanoparticles, as a function of nanoparticle size and surface functionalization, cells are incubated at 37 °C with nanoparticle suspensions at the final concentrations described above.
2. After 24 hours incubation, cells are rinsed with PBS and lysed with 100 µl of 1% Triton X100 in PBS.
3. Cell lysates are analyzed by a spectrofluorometer (Wallac 1420 Victor2, Perkin–Elmer, USA) to measure the fluorescence intensity of internalized nanoparticles.

4. Nanoparticle concentration in the samples is determined by interpolating the fluorescence intensity data of the samples with the calibration curve and normalized to cell number.

3.7.2. Nanoparticle transcytosis experiments

The permeability experiments are performed on the monolayer 7 days after cell seeding, allowing sufficient time for the cells to develop the tight junctions (Figure 6).

1. On the day of experiment, prepare the nanoparticle suspension by diluting nanoparticle stock in complete media w/o phenol red as described above.
2. Remove the media and wash the Transwell insert filter where cells are seeded with PBS with Ca^{2+} and Mg^{2+} (Gibco) to eliminate traces of phenol red that could affect fluorescence measurements.
3. Then, fill first the donor chamber with 0.15 ml complete medium w/o phenol red containing nanoparticles and second the acceptor chamber with 0.4 ml complete medium w/o phenol red (Figure 2).
4. Collect the samples of 0.4 ml every 10 min for 90 min from the acceptor chamber and then replace them with the same amount of complete medium w/o phenol red.
5. Measure the fluorescence intensity of the samples by spectrophotometer. The excitation and emission wavelengths are set to 485 and 535 nm, respectively, for all fluorescence tracers in the present study.
6. At the end of 90 min, wash the filter and fill first the donor chamber with 0.15 ml complete medium without phenol red containing 0.5 mg/ml BSA and second the acceptor chamber with 0.4 ml complete medium w/o PR.

7. Repeat step 4 and 5.
8. To have a statistical significance, the experiments should be performed in triplicate at least.

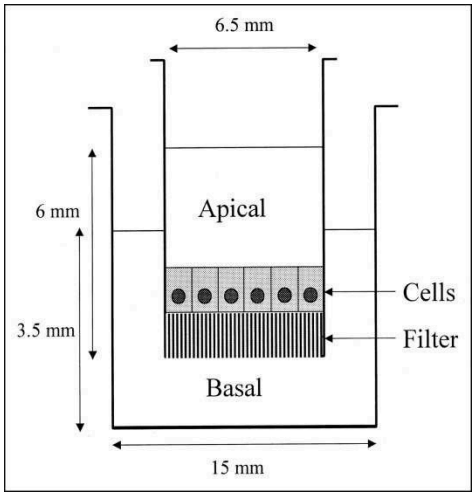

Figure4. Schematic representation of a blood-brain barrier in vitro model on transwell

3.8.3. Calculation of nanoparticle concentration in the acceptor chamber

Nanoparticle concentration in the samples is determined by interpolating the fluorescence intensity data of the samples with the calibration curve.

1. For the calibration curve, prepare a 1:2 dilution series of nanoparticle standards in the concentration range of $0 – 3.6 \times 10^{10}$ NP/ml by diluting the nanoparticle stocks in cell culture media w/o phenol red.
2. Sonicate nanoparticle suspensions for 5 min at room temperature in ultrasonic bath.
3. Transfer 100 µl of each nanoparticle standard to a 96-well plate suitable for fluorescence measurement.
4. Read the fluorescence with a fluorescence plate reader at 488 nm excitation /530 nm emission for green and orange fluorescent nanoparticles and at 543 nm excitation /560 nm emission for red fluorescent nanoparticles.

5. Transport of nanoparticles across the BBB depends on nanoparticle size and surface charge. In particular, smaller (NP44) and positively charged (NP-NH_2) nanoparticles are transported more efficiently through the endothelial layer than NP100 and NP-COOH (Figure 5)

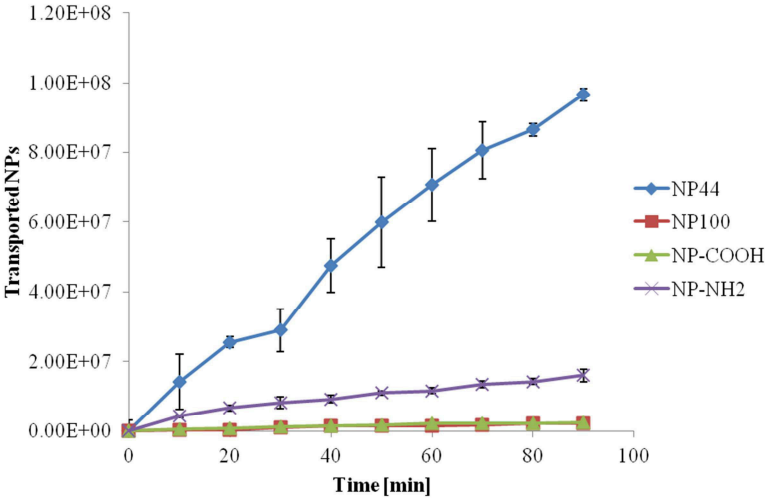

Figure 5. Transport of nanoparticles across blood-brain barrier

3.8.4. Calculation of permeability

The solute permeability (P) of the monolayer is calculated from the relationship,

$$P = \frac{\frac{\Delta C_A}{\Delta t} \times V_A}{C_D \times S}$$

where $\Delta C_A/\Delta t$ is the increase in fluorescence concentration in the accepter chamber during the time interval Δt, C_D is the fluorescence concentration in the donor chamber (assumed to be constant during the experiment), V_A is the volume of the acceptor chamber, and S is the surface area of the filter.

3.8.5. Confocal microscopy analysis of Transwell filters after permeability experiments

Confocal microscopy observations are carried out to verify the integrity of the endothelial layer and the presence of nanoparticles within the cells (Figure 4).

1. After 90 minute incubation with nanoparticles, wash twice the filter with PBS to remove excess of nanoparticles.
2. Fix the cells with 4% paraformaldeyhde in PBS for 20 min at room temperature.
3. After fixation, wash the samples with PBS.
4. Incubate the cells with fluorescent WGA solution in PBS for 10 min at room temperature to stain cell membranes.
5. After incubation, wash twice the samples with PBS.
6. Cut the filter from the Transwell support with a scalpel and wash it with Milli-Q water.
7. Remove excess of water by gently drying the filter with paper.
8. Mount the filter on a glass slide with PBS/glycerol (1:1) solution and cover it with a glass coverslip.
9. Observe the samples by the confocal microscope.

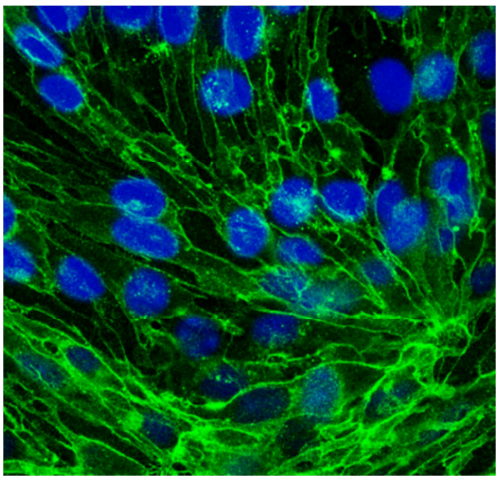

Figure 6. Claudin(Green) and Dapi (blue).bEnd3 cell line.

References

1. E. Neuwelt, N. J. Abbott, L. Abrey, W. A. Banks, B. Blakley, T. Davis, B. Engelhardt, P. Grammas, M. Nedergaard, J. Nutt, W. Pardridge, G. A. Rosenberg, Q. Smith and L. R. Drewes, *Lancet Neurol.* **2008** *7*, 84.
2. N. J. Abbott, L. Ronnback and E. Hansson, *Nat. Rev. Neurosci.* **2006** *7*, 41.
3. G. Tosi, L. Costantino, F. Rivasi, B. Ruozi, E. Leo, A. V. Vergoni, R. Tacchi, A. Bertolini, M. A. Vandelli and F. Forni, *J. Control. Release* **2007** *122*, 1.
4. J. Kreuter, *Adv Drug Deliv Rev* **2001** *47*, 65.
5. S. V. Dhuria, L. R. Hanson and W. H. Frey, 2nd, *J. Pharm. Sci.* **2010** *99*, 1654.
6. a)B. DiBlasio, S. Galdiero, M. Saviano, G. DeSimone, E. Benedetti, C. Pedone, W. A. Gibbons, R. Deschenaux, E. Rizzarelli and G. Vecchio, *Supramolecular Chemistry* **1996** *7*, 47; b)D. Paolino, D. Cosco, R. Molinaro, C. Celia and M. Fresta, *Drug Discov. Today* **2011** *16*, 311; c)H. Yang, *Pharm. Res.* **2010** *27*, 1759.
7. E. Garcia-Garcia, K. Andrieux, S. Gil and P. Couvreur, *Int. J. Pharm.* **2005** *298*, 274.
8. J. C. Olivier, *NeuroRx* **2005** *2*, 108.
9. J. C. Olivier, *NeuroRx* **2005** *2*, 108.
10. M. Zorko, U. Langel, *Adv. Drug Deliv. Rev.* **2005** *57*, 529.
11. S. Deshayes,M. C.Morris, G. Divita, F. Heitz, *CellMol. Life Sci.***2005** *62*, 1839.
12. L. Liu, S. S. Venkatraman, Y. Y. Yang, K. Guo, J. Lu, B. He, S. Moochhala, L. Kan, *Biopolymers* **2008** *90*, 617.
13. a) S. Galdiero, M. Vitiello, A. Falanga, M. Cantisani, N.Incoronato, M. Galdiero, *Curr. Drug Metab.* **2012***13*, 93; b) A.Falanga, M. Cantisani, C. Pedone, S. Galdiero, *Protein Pept.Lett.* **2009***16*, 751; c) S. Galdiero, A. Falanga, M. Vitiello, M. D'Isanto, C. Collins, V. Orrei, H. Browne, C. Pedone, M. Galdiero, *ChemBioChem* **2007***8*, 885; d) S. Galdiero, M.

Vitiello, M. D'Isanto, A. Falanga, M. Cantisani, H. Browne, C. Pedone, M. Galdiero, *ChemBioChem* **2008***9*, 758.

14. a) G. Vitiello, A. Falanga, M. Galdiero, D.Marsh, S. Galdiero, G. D'Errico, *Biochim. Biophys. Acta* **2011***1808*, 2517; b) S. Galdiero, A. Falanga, M. Vitiello, M. D'Isanto, M. Cantisani, A. Kampanaraki, E. Benedetti, H. Browne, M. Galdiero, *Peptides* **2008***29* 1461; c) S. Galdiero, A. Falanga, G. Vitiello, M. Vitiello, C. Pedone, G.D'Errico, M. Galdiero, *Biochim. Biophys. Acta* **2010***1798*, 579; d) S. Galdiero, A. Falanga, M. Vitiello, L. Raiola, L. Russo, C. Pedone, C. Isernia, M. Galdiero, *J. Biol. Chem.* **2010***285*, 17123; e) S. Galdiero, A. Falanga, M. Vitiello, L. Raiola, R. Fattorusso, H. Browne, C. Pedone, C. Isernia, M. Galdiero, *J. Biol. Chem.* **2008***283*, 29993; f) S. Galdiero, A. Falanga, M. Vitiello, H. Browne, C. Pedone, M. Galdiero, *J. Biol. Chem.* **2005***280*, 28632.

15. a) A. Falanga, M. T. Vitiello, M. Cantisani, R. Tarallo, D. Guarnieri, E. Mignogna, P. Netti, C. Pedone, M. Galdiero, S. Galdiero, *N nomedicine* **2011***7*, 925; b) R. Tarallo, A. Accardo, A. Falanga, D. Guarnieri, G. Vitiello, P. Netti, G. D'Errico, G. Morelli, S. Galdiero, *Chemistry* **2011***17*, 12659; c) T. P. Carberry, R. Tarallo, A. Falanga, E. Finamore, M. Galdiero, M. Weck, S. Galdiero, *Chemistry* **2012**,

16. a) R. C. Brown, A. P. Morris and R. G. O'Neil, *Brain Res.* **2007** *1130*, 17; b)Y. Omidi, L

17. Barrier, B. B. (2010). Blood–brain barrier. *Cancer Symptom Science: Measurement, Mechanisms, and Management*, 9.

18. Janzer, R. C., & Raff, M. C. (1987). Astrocytes induce blood–brain barrier properties in endothelial cells. *Nature*, *325*(6101), 253-257.

19. Kniesel, U., & Wolburg, H. (2000). Tight junctions of the blood–brain barrier. *Cellular and molecular neurobiology*, *20*(1), 57-76.

20. Huber, J. D., Egleton, R. D., & Davis, T. P. (2001). Molecular physiology and pathophysiology of tight junctions in the blood–brain barrier. *Trends in neurosciences*, *24*(12), 719-725.